Chemical Science

ROYAL SOCIETY OF CHEMISTRY

REVIEW

View Article Online
View Journal | View Issue

Cite this: *Chem. Sci.*, 2024, **15**, 3071

Advancements in aqueous zinc–iodine batteries: a review

Zhongchao Bai, †[a] Gulian Wang,†[b] Hongmin Liu,†[a] Yitao Lou,†[a] Nana Wang,*[c] HuaKun Liu[a] and Shixue Dou *[a]

Aqueous zinc-iodine batteries stand out as highly promising energy storage systems owing to the abundance of resources and non-combustible nature of water coupled with their high theoretical capacity. Nevertheless, the development of aqueous zinc-iodine batteries has been impeded by persistent challenges associated with iodine cathodes and Zn anodes. Key obstacles include the shuttle effect of polyiodine and the sluggish kinetics of cathodes, dendrite formation, the hydrogen evolution reaction (HER), and the corrosion and passivation of anodes. Numerous strategies aimed at addressing these issues have been developed, including compositing with carbon materials, using additives, and surface modification. This review provides a recent update on various strategies and perspectives for the development of aqueous zinc-iodine batteries, with a particular emphasis on the regulation of I_2 cathodes and Zn anodes, electrolyte formulation, and separator modification. Expanding upon current achievements, future initiatives for the development of aqueous zinc-iodine batteries are proposed, with the aim of advancing their commercial viability.

Received 16th November 2023
Accepted 22nd January 2024

DOI: 10.1039/d3sc06150g

rsc.li/chemical-science

1. Introduction

The growing demand for energy in society has motivated scientists to delve into innovative research on new energy sources and storage solutions.[1,2] Electrochemical energy storage is a crucial area of research, and lithium-ion batteries (LIBs), one of its representative technologies, have found widespread applications in the everyday lives of people. However, their production costs, safety problems, and the environmentally unfriendly nature of organic electrolytes have prompted researchers to develop partial alternatives to LIBs.

Aqueous zinc-based batteries are considered to be one of the most promising systems owing to the abundance of zinc resources and the non-combustible nature of water combined with the high theoretical capacity (820 mA h g^{-1}, 5855 mA h cm^{-3}), low electrode potential (−0.76 V *versus* standard hydrogen electrode (SHE)), and air stability of Zn.[3–8] In recent years, aqueous zinc-based secondary batteries have been significantly developed; however, it is difficult to match them with suitable cathodes. Instances abound where commonly employed cathodes such as MnO_2 (ref. 9) and V_2O_5 (ref. 10) encounter challenges related to lattice structure distortion, collapse, and the dissolution of active species during cycling processes, contributing to a rapid decline in capacity over cycles. When polyaniline (PANI) serves as a cathode, its specific capacity in a mildly acidic electrolyte is usually limited to no more than 100 mA h g^{-1}.[11] While choosing sulfur (S) as a cathode, it will lead to a notably low discharge platform of Zn–S batteries, typically about 0.8 V.[12] In comparison, an iodine cathode stands out as an excellent choice. I_2 exhibits a high theoretical specific capacity of 211 mA h g^{-1} and can achieve a discharge platform of nearly 1.3 V when paired with a zinc anode. Furthermore, in comparison to the previously mentioned cathodes, zinc-iodine batteries demonstrate exceptional cycling performance, often sustaining stability over thousands of cycles. Additionally, the polyvalent properties of iodine elements such as I^+ and I^{5+}, can contribute to higher cathode capacities.[13–16]

Zinc-iodine batteries can be classified into zinc-iodine redox flow batteries (ZIRFBs) and static zinc-iodine batteries (SZIBs). Specifically, SZIBs have a simpler structure compared to ZIRFBs, such as the omission of tanks and pumps, and have attracted increasing attention in the last two years.[17] Hence, our focus is exclusively on the development of stationary zinc-iodine batteries in this review. Nevertheless, the development of zinc-iodine batteries has consistently faced challenges associated with iodine cathodes and zinc anodes. For the cathode side, the electronic insulation property of I_2 will increase the polarization of batteries; the formed polyiodine ions will shuttle to the anode and cause self-discharge phenomenon; the limited active

[a]*Institute of Energy Materials Science (IEMS), University of Shanghai for Science and Technology, 516 Jungong Road, Shanghai, 200093, China. E-mail: shi@uow.edu.au*
[b]*Key Laboratory of Colloid and Interface Chemistry, Ministry of Education, School of Chemistry and Chemical Engineering, Shandong University, Jinan 250100, PR China*
[c]*Institute for Superconducting and Electronic Materials, Australian Institute for Innovative Materials, Innovation Campus, University of Wollongong, Squires Way, North Wollongong, NSW 2500, Australia. E-mail: nanaw@uow.edu.au*
† These authors contributed equally to this work.

materials content is not conducive to achieving high energy density. For the Zn anode side, besides suffering from corrosion by polyiodide ions, it also faces dendrites, hydrogen evolution, and water-related corrosion and passivation problems. Moreover, when these issues are mixed together, the situation is more complicated. In addressing these challenges, researchers have undertaken substantial efforts, for instance, designing porous carbon material hosts to limit iodine species and improve iodine utilization, developing new electrolytes to inhibit the production of polyiodine intermediates, exploiting functional separators to suppress polyiodine ions shuttling, and constructing coating layers on anode to protect Zn metal.

Substantial strides have been made in the advancement of zinc-iodine batteries and relevant papers have been increasing, especially in the years 2022 and 2023. It is further noted that the number of articles published in 2023 is nearly twice that in 2022 (according to the results of Web of Science search on the topic of "zinc-iodine batteries"). Nevertheless, the corresponding comprehensive review articles are few, and most were published before 2023. In order to stay abreast of the latest research developments, a real-time review is imperative. In this manuscript, we conduct a comprehensive analysis of the current research progress on SZIBs (Fig. 1). Firstly, the energy storage mechanism and key challenges were introduced, and then research situations on cathodes, anodes, electrolytes, as well as separators were systematically introduced and analyzed. Finally, we present additional conclusions and prospects, aiming to contribute to the development of SZIBs.

1.1 The working mechanism of SZIBs

SZIBs can be classified into two types based on the iodine sources.[18,19] A conventional structure is depicted in Fig. 2a, wherein I_2 serves as the source of active species. In this case, the cathode is usually prepared using carbon-based materials with large specific surface area or porous structure as the host to encapsulate I_2 by means of melt infiltration or immersion.[20,21] The zinc-iodine battery works based on the chemical conversion reaction of I_2 cathode and the deposition/stripping reaction of Zn anode. Specifically, during the discharging process, I_2 gets

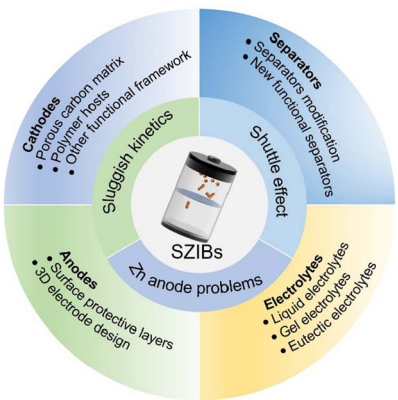

Fig. 1 Overview of challenges in and improved strategies for constructing aqueous zinc-iodine batteries.

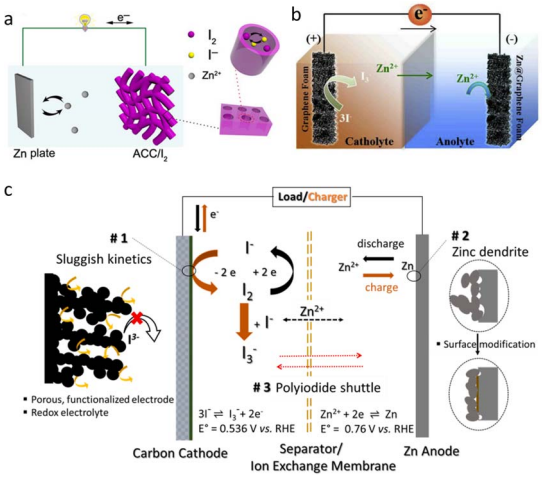

Fig. 2 (a) The structure of SZIBs with I_2 as the source of iodine. Reproduced with permission.[18] Copyright 2018, Springer. (b) The structure of SZIBs with I_3^- or I^- in electrolytes as the source of iodine. Reproduced with permission.[19] Copyright 2019, Elsevier. (c) The schematic illustration of the limitations of SZIBs. Reproduced with permission.[22] Copyright 2023, Elsevier.

electrons and is reduced to I^-, while Zn loses electrons and is oxidized to Zn^{2+}, *i.e.*, the stripping process of Zn. Moreover, the generated I^- can further react with I_2 to form I_3^-, and the I_3^- has a chance to be reduced to I^- again. The charging process is conversely. The corresponding equations are as follows.

$$\text{Anode: } Zn^{2+} + 2e^- \leftrightarrow Zn,\ E = -0.763\ \text{V } \textit{vs.}\ \text{SHE} \quad (1)$$

$$\text{Cathode: } I_2 + 2e^- \leftrightarrow 2I^-,\ E = 0.535\ \text{V } \textit{vs.}\ \text{SHE} \quad (2)$$

$$I^- + I_2 \leftrightarrow I_3^- \quad (3)$$

$$I_3^- + 2e^- \leftrightarrow 3I^-,\ E = 0.536\ \text{V } \textit{vs.}\ \text{SHE} \quad (4)$$

$$\text{Overall: } I_2 + Zn \leftrightarrow Zn^{2+} + 2I^-,\ E = 1.298\ \text{V} \quad (5)$$

$$Zn + I_3^- \leftrightarrow Zn^{2+} + 3I^-,\ E = 1.299\ \text{V} \quad (6)$$

However, this kind of cathodes has low active material contents (currently, most are less than 50%), which is mainly due to the poor electron-conductivity of I_2. In addition, the high volatile nature of I_2 also poses challenges for its preparation and application.

Another SZIBs structure is shown in Fig. 2b, in which I_3^- or I^- in electrolytes provide iodine source for electrochemistry reaction, and the cathodes are usually carbon-based materials with adsorption ability, similar to ZIRFBs.[23,24] When discharging, the I_3^- will get electrons and be reduced to I^- at the cathode-electrolyte interface and a stripping process happens at the Zn anode, simultaneously. The charging process is converse. The corresponding anode reaction can also be described using eqn (1), the cathode reactions can be expressed as eqn (4), and the overall reaction can be illustrated as eqn (6). The presence of iodine source in this way can provide more

active substance content, but the disadvantage is that the reaction usually occurs at the interface, and the inner space of the cathode is not sufficiently utilized. Moreover, the active substance amount is related to the electrolyte volume, which is not conducive to the improvement of the volume energy density, especially when the battery is amplified.

It should be emphasized that in both the types, the involvement of iodine is limited to the conversion between I_3^-, I^-, and I_2. The resulting capacity and discharge voltage are constrained, posing a challenge to achieving high energy density. Fortunately, iodine also has higher valence states like +1, +5, and +7. This means that activating these valence states can realize more electrons transfer, thereby enabling higher energy density. Currently, the primary focus of this research is on the conversion involving $I^-/I_2/I^+$ as the higher valence states pose greater challenges.[15] Moreover, in $I^-/I_2/I^+$ conversion, the element of chlorine (Cl) is usually introduced to stabilize I^+.[14] The anode reaction during this conversion can still be illustrated by eqn (1). For the cathode side, the I^-/I_2 stage can be expressed by eqn (2) and I_2/I^+ stage can be described by

$$I_2 + 2Cl^- \leftrightarrow 2ICl + 2e^-,\ E = 1.07\ V\ vs.\ SHE \quad (7)$$

Therefore, the total reactions are eqn (5) and

$$Zn^{2+} + I_2 + 2Cl^- \leftrightarrow Zn + 2ICl,\ E = 1.83\ V \quad (8)$$

1.2 The challenges for SZIBs

Despite the promising prospects of SZIBs, there are still some challenges that need to be addressed at the current stage (Fig. 2c). One of the biggest challenges facing the SZIBs is the polyiodine ions' formation.[23] Just as mentioned above, during the working process, both the two types of SZIB will generate I_3^- and can further coordinate with I_2 to form I_5^-, and I_5^- can coordinate with I_2 to form I_7^-. The polyiodide ions, being highly water-soluble, tend to shuttle through the separator toward the anode side due to the concentration gradient, *i.e.*, "shuttle effect". A direct result of this phenomenon is Zn corrosion because polyiodine ions can react with Zn metal ($Zn + I_3^- \rightarrow Zn^{2+} + 3I^-$ + heat). In addition, the electron transfer in this reaction is not going through the external circuit, which will result in a serious self-discharge problem, thus lowering the coulombic efficiency (CE). Another challenge of the system is the problem of sluggish kinetics.[22] The insulated I_2 and other iodine species greatly impede the efficient transport of electrons, which will lead to a slow charge transfer. In this context, increasing the amount of carbon is necessary to enhance the electron conductivity; however, this improvement is constrained and may lead to a reduction in battery energy density. In addition to the sluggish electron transfer, the sluggish kinetics can also be related to the slow mass transfer process. The mass transfer is often associated with the efficiency of ionic transport. The low ionic conductivity of electrolytes and separators further contributes to these challenges.[17,25]

Besides cathodes, the Zn metal anode also face great challenge, and numerous studies have been done to improve it in recent years.[26,27] In addition to the severe corrosion caused by polyiodine ions, zinc also encounters challenges such as dendrite formation, HER, corrosion from water, and passivation. Specifically, the reduced zinc ions are intended to accumulate at protrusions due to the "tip effect" and gradually evolve into dendrites. The dendrites have the risk of puncturing separators and causing short circuits. Moreover, some dendrites will break away from the Zn anode, becoming "orphan" or "dead" Zn, which leads to a loss of active zinc and a low CE.[28] Besides, it's worth noting that zinc metal is not thermodynamically stable in water, and the HER competes strongly with Zn reduction. Despite the presence of an overpotential, the reaction cannot be entirely circumvented, and the produced H_2 can lead to battery swelling and failure. Concurrent with H_2 evolution is the corrosion of zinc as this parasitic reaction unfolds eqn (9) and (10).

$$\text{positive electrode: } 2H^- + 2e^- \rightarrow H_2 \quad (9)$$

$$\text{negative electrode: } Zn - 2e^- \rightarrow Zn^{2+} \quad (10)$$

The generation of H_2 also implies the decomposition of H_2O, leading to an elevated concentration of OH^- in the vicinity of the zinc metal. This, in turn, results in the production of inert by-products, such as basic zinc sulfate, which can deactivate the zinc anode. More importantly, these unfavorable factors affect each other, thus aggravating the deterioration of zinc anode condition.[29]

2. Cathode materials for SZIBs

In the realm of rechargeable battery systems, aqueous SZIBs have attracted widespread attention due to their significant advantages stemming from elemental iodine. This includes high theoretical capacity (211 mA h g^{-1}), high redox potential (I_2/I^-, 0.536 V *vs.* SHE), and the ability to match with the Zn anode.[17,30] However, the inherent physicochemical properties of I_2 have a negative effect on the electrochemical performance of aqueous SZIBs batteries. Firstly, the poor conductivity of solid I_2 results in sluggish cathodic redox kinetics. Secondly, solid I_2 exhibits poor thermal stability and is easy to sublimate. Additionally, during the charging process, the polyiodide generated by the oxidation of iodine continuously dissolves in the electrolyte, resulting in a shuttle effect.[31] These issues lead to a rapid capacity reduction, high self-discharge rate, and poor coulombic efficiency.[17] Therefore, it is imperative to develop high-performance cathode materials capable of accommodating I_2. This endeavor encompasses a broad range of materials, including porous carbon matrix (carbon fiber cloth,[18] carbon nanotubes/sheets/shells,[32–34] graphene,[19] heteroatom-doped carbon materials,[35–38] biomass carbon[39]), polymers,[40] functional framework structures (metal–organic frameworks,[41,42] covalent-organic frameworks, Mxene[43] and perovskite unit structures), and complex materials.[44,45] The overarching objective is to enable the efficient utilization of iodine, inhibit the polyiodide shuttle effect, and thus enhance the performance of SZIBs. When designing cathode materials, several key factors

should be taken into consideration: (1) iodine carriers must possess high electronic conductivity and ample porosity, which can enhance the iodine adsorption and the conversion reaction *via* the physicochemical confinement effect, thus preventing "shuttle effect" and self-discharge; (2) the regulation of surface properties and structure in porous carbon materials is critical for enhancing the adsorption of iodine substances, thereby improving the reversibility of batteries; (3) the synergistic effect of each component in complex materials is essential for improving the output voltage and energy density of SZIBs batteries.

2.1 Porous carbon matrix

Porous carbon materials possess a unique set of characteristics, including a robust skeleton, high conductivity, and abundant porosity, making them ideal for the storage of substantial quantities of iodine. As shown in Fig. 3a, Li *et al.*[46] encapsulated iodine in porous activated carbon through simple physical adsorption. This ingenious approach effectively inhibited the dissolution of polyiodide and ensured cycling stability. Meanwhile, the porous conductive carbon matrix promoted the conversion reaction between I_2 and ZnI_2. Consequently, the electrochemical performance of SZIBs has been improved substantially, including a capacity of 210 mA h g^{-1}, an energy density of 237 W h kg^{-1}, and an energy efficiency of 96.7% at 100 mA g^{-1} (Fig. 3b). The pore size of activated carbon, however, is relatively large (5 μm), which facilitates the aggregation of iodine on the surface of these macroporous activated carbons and consequently hinders the efficient conversion of polyiodide and leads to their dissolution in the electrolyte. In order to achieve high-quality iodine loading, Guo *et al.*[47] selected a mesoporous carbon structure with a pore diameter of 50 nm for the adsorption of iodine (I_2/CMKs), thereby enhancing the performance of SZIBs (Fig. 3c). The synthesized I_2/CMKs composites effectively restricted the I_3^-/I^- conversion reaction within the pores and eliminated the shuttle effect caused by polyiodide, resulting in significantly improved cycle stability (Fig. 3c). The battery exhibited a specific capacity of 90 mA h g^{-1} at a high current density of 5 A g^{-1} and an impressive longevity with 39 000 ultra-long cycles achieved at 10 A g^{-1} with a remarkable capacity retention rate of 80.6% (Fig. 3d). Moreover, the spatial architecture of microporous carbon materials with pore sizes of 1–3 nm is highly matched with the spatial arrangement of iodine, thus establishing an effective confinement mechanism for achieving high-quality I_2 loading. Hou *et al.*[48] clearly elucidated the important contribution of the ~2.5 nm pore structure of nanocarbon to I_2 adsorption and rapid polyiodide conversion through the intelligent synthesis method of H-bond-gifted uniform precursor and the precise coordination of different pore-forming agents. The enhanced adsorption efficiency of I_2, facilitated rapid conversion of I^-/I_2, and suppressed iodide dissolution can be attributed to the presence of a 2.5 nm pore structure in carbon material. Additionally, a novel mechanism was developed to investigate the

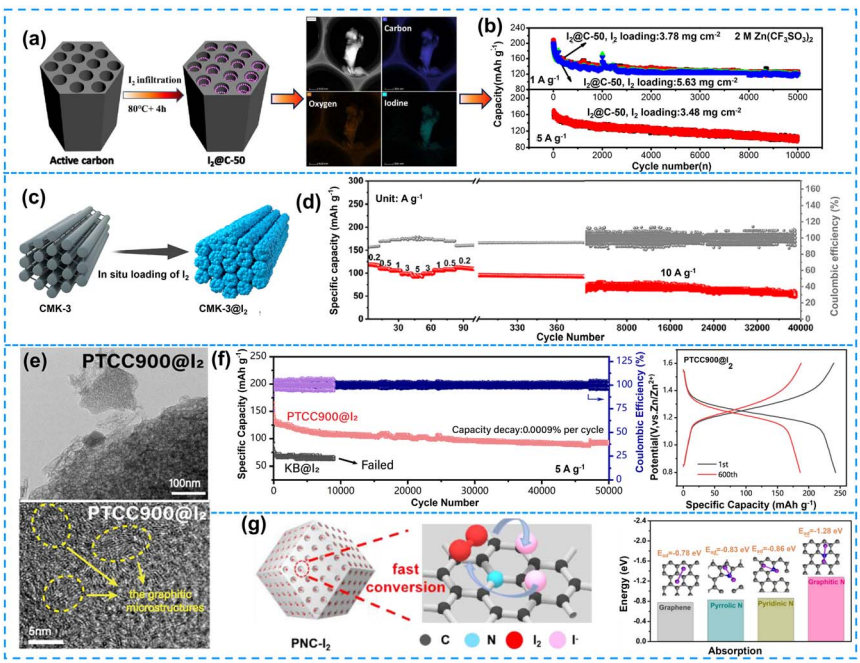

Fig. 3 (a) Synthetic illustration of I_2@C-50 composites, TEM elemental mapping of the I_2@C-50 composite. (b) Cycling performance of I_2@C-50 composite with different I_2 mass loading at a current density of 1 and 5 A g^{-1}. Reproduced with permission.[46] Copyright 2020, the Royal Society of Chemistry. (c) Schematic illustration of the preparation of CMK-3@I_2. (d) Rate capability and cycling stability of the zinc-iodine battery. Reproduced with permission.[47] Copyright 2022, American Chemical Society. (e) SEM images of PTCC900@I_2. (f) Long cycling stability and CE of PTCC900@I_2 under a large current density of 5 A g^{-1}, GCD curves of PTCC900@I_2. Reproduced with permission.[49] Copyright 2023, Elsevier. (g) Schematic illustration of the preparation process of N-doped porous carbons. Binding energies between I_2 and graphene, pyrrolic N, pyridinic N, and graphitic N. Reproduced with permission.[52] Copyright 2022, Elsevier.

correlation between pore structure and cathodic iodine oxidation for achieving optimal zinc-iodine battery performance.

To further elucidate the impact of pore size on the adsorption and conversion of I_2, graded porous structures can be employed to achieve a homogeneous distribution of micropores and mesopores with varying sizes on the surface, thereby effectively enhancing iodine loading. Wu *et al.*[49] reported the synthesis of a perylene-3,4,9,10-tetracarboxylic anhydride (PTCDA)-based carbon host (PTCC900) through annealing at 900 °C to effectively confine iodine species. PTCC900 exhibited a hierarchical porous structure with a pore size ranging from 1.8 to 13 nm, which facilitated the encapsulation of I_2 and polyiodide species. As illustrated in Fig. 3e, the distribution of iodine was predominantly observed within micropores and in the presence in mesopores as well. Moreover, the incorporation of vortex layer graphite microstructure within PTCC900 not only provided a rapid pathway for electron transfer but also enhanced its conductivity. At a current density of 0.5 A g^{-1}, an initial capacity of 240 mA h g^{-1} was achieved by the PTCC900@I_2 cathode material. Remarkably, even when subjected to higher current densities such as 5 A g^{-1}, the PTCC900@I_2 cathode demonstrated exceptional cycling stability exceeding 50 000 cycles (Fig. 3f). Therefore, the synergistic combination of micropores and mesopores not only enables the uniform loading of I_2 but also facilitates efficient ion transport within the electrolyte matrix, leading to SZIBs with high capacity and prolonged cycle life.

To further advance the development of cost-effective and highly porous carbon materials, Xu *et al.*[37] designed a biomass-derived hierarchically porous carbon as an iodine host material for high-performance SZIBs. The hierarchically porous structure exhibited high specific surface area, which not only provided a rich channel for electrolyte infiltration but also physically confined the I_2 during cycling. These properties enhanced iodine utilization, accelerated reaction kinetics, and resulted in excellent cycle stability and high coulombic efficiency for SZIBs. A high discharge capacity of 100 mA h g^{-1} was still retained for over 150 cycles at a current density of 100 mA g^{-1}. Han *et al.*[50] developed activated porous corncob carbon (APCC) with high surface area, conductivity, and adsorption capacity as an effective iodine carrier. Additionally, employing $ZnCl_2$ electrolyte support, the battery achieved a higher voltage platform for the conversion reaction involving $I^-/I^0/I^+$ four electron transfer mechanism, which significantly differed from the conventional static zinc-iodine battery (I^-/I^0). Ultimately, the specific capacity of the battery reached 1118.6 mA h g^{-1} while attaining an energy density of 1302.2 W h kg^{-1}. The development of biomass-derived carbon offers a green, renewable, and straightforward approach for fabricating high-performance main materials in SZIBs.

The porous carbon materials, serving as the host material of I_2, possess several advantages including wide availability, high electrical conductivity, good chemical stability, and rich porosity.[51] However, the polar-nonpolar adsorption force between porous carbon and iodine is weak, not conducive to restraining iodine species. Hence, grafting of polar functional groups or heteroatomic doping strategies are often used.

To further enhance the adsorption of I_2 on porous carbon materials and improve the energy density and power density of aqueous SZIBs, a heteroatom doping strategy was introduced. The heteroatom-doped carbon matrix alters the state of carbon charge density, increasing the probability of defects and exposing more active sites. Furthermore, the synergistic effect between heteroatoms and porous carbon materials enhances the redox kinetics of I_2.[21] Importantly, the doped elements (such as N, S, P, Fe,[53] Ni, and FeN[54]) and the ability to provide binding sites are decisive factors affecting iodine adsorption. Liu *et al.*[52] achieved a high energy density (320 W h kg^{-1}) and ultra-long cycle life (10 000 cycles) aqueous zinc-iodine battery by catalyzing iodine with N-doped porous graphene carbon while inhibiting the dissolution of triiodides (Fig. 3g). This was mainly attributed to the electron redistribution from graphitic N in carbon to iodine molecules after interaction, which enhanced the iodine adsorption capacity. It not only enhanced the redox conversion efficiency in thermodynamics but also facilitated the conversion of I_3^-/I^- in kinetics by reducing the dissociation energy barrier. Dang *et al.*[22] further demonstrated the high surface area and conductivity of N-doped graphene structure, which significantly facilitated iodide redox reactions and restricted polyiodide formation, thereby resulting in enhanced power and energy density. Moreover, anchoring the unique coordination structure of transition metal atoms and heteroatoms (usually nitrogen, M–N–C) onto a carbon substrate can effectively achieve high utilization and excellent activity of iodine (Fig. 4a).[44,55] It is worth

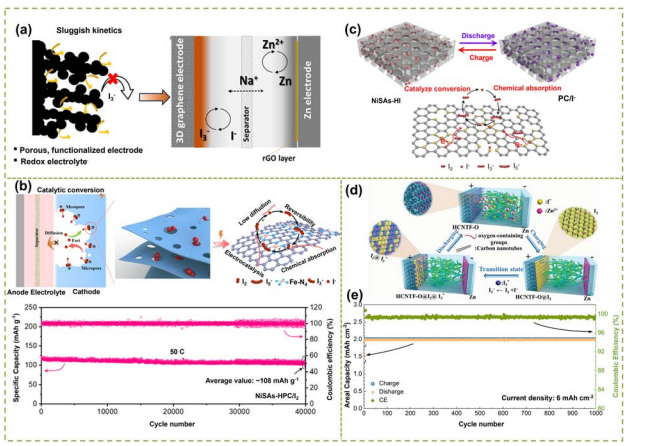

Fig. 4 (a) Schematic representation of a conventional zinc-iodine battery of a three-dimensional functionalized graphene cathode. Reproduced with permission.[22] Copyright 2023, Elsevier. (b) Schematic illustration for the proposed reaction mechanism of polyiodide adsorption/conversion on the matrix of B–Fe–NC; long-term cycling performance of B–Fe–NC/I_2 at 10C. Reproduced with permission.[20] Copyright 2022, American Chemical Society. (c) Schematic illustration of the discharge/charge behavior of SZIBs using NiSAs-HPC/I_2 cathodes. Reproduced with permission.[56] Copyright 2023, American chemical society. (d) Schematic illustrations of the operation mechanism of the ZIDMBs. Reproduced with permission.[57] Copyright 2022, Wiley-VCH. (e) Capacity and coulombic efficiency evolution during long-term cycling at 6 mA cm^{-2}. Reproduced with permission.[58] Copyright 2022, Elsevier.

noting that minimizing atom dispersion on the surface of metal atoms in heteroatom coordination structures plays a crucial role in improving the structural stability. Liu *et al.*[20] embedded a single iron atom in porous carbon using an M–N–C atomic bridging structure, which enhanced the high-quality loading of iodine and effectively promoted ion diffusion (Fig. 4b). Meanwhile, the DFT revealed that the distinctive atomic bridging structure of Fe–N_4–C in B–Fe–NC not only enhances the chemical capture for iodine species but also facilitates the redox reaction of iodine. Consequently, the zinc-iodine battery exhibited a substantial capacity and excellent cycle stability. In addition, in order to further improve the loading rate of iodine and suppress the shuttle effect, metal atoms are embedded into layered porous carbon. For example, Ma *et al.*[56] enhanced the loading rate of iodine by uniformly dispersing Ni single atoms (NiSAs) onto hierarchical porous carbon frameworks (NiSAs-HPC), as illustrated in Fig. 4c. *In situ* Raman analysis further confirmed the remarkable electrocatalytic activity of NiSAS-HPC on polyiodides. The high pore volume facilitated efficient iodine loading, while the hierarchical microporous structure prevented dissolution and the possible shuttle effect of polyiodide. Impressively, the assembled zinc-iodine battery exhibited excellent rate capability (121 mA h g^{-1} at 50C) and ultra-long cycling stability (over 40 000 cycles at 50C).

Additionally, the optimization of surface functional groups on carbon materials and the construction of hierarchical porous structures also exerts positive effects on both the anchoring effect and redox reaction of active materials. Zhang *et al.*[59] used a high-density ordered porous graphene (HOPG) as the iodine host. The HOPG has a large amount of micropores and higher specific surface area owing to the KOH etching of GO during the preparation process, which can accommodate more active species. Meanwhile, more oxygen-containing functional groups were introduced, providing more sites for binding polyiodides. Ji *et al.*[60] employed a high-efficiency electroplating technique to load I_2 onto the rGO electrode, thereby circumventing any loss of active material caused by the thermal instability of I_2 and significantly suppressing the shuttle effect of iodine. The performance of battery was significantly enhanced, exhibiting a remarkable CE of up to 95% and demonstrating exceptional cycle stability with nearly 100% capacity retention after 2000 cycles at 50 mA cm^{-2}. In addition, Liu *et al.*[61] incorporated graphene quantum dots into graphite felt to fabricate a highly stable static zinc-iodine redox battery. The surface functional groups of graphene quantum dots were utilized to regulate the oxidation and complexation of I_2 and ZnI_2, thereby enhancing the performance of static zinc-iodine redox batteries. Besides graphene, Jin *et al.*[57] utilized laser direct writing technology to fabricate hydrophilic carbon nanotube (HCNT-O) cathodes with abundant oxygen-containing functional groups. As shown in Fig. 4d, the carbon nanotube structure and abundant oxygen functional groups in HCNT-O facilitated the electro-deposition of I^-/I_3^- on the cathode surface, effectively alleviating the shuttle effect of I_3^-. Therefore, the aqueous zinc-iodine battery exhibited a significant volume of 1647.3 mW h cm^{-3} and a high energy density of 2339.1 μW h cm^{-2}. To further explore the effects of oxygen functional groups and pore structures on the electrochemical charge storage capacity of SZIBs, Chen *et al.*[62] reported a porous oxidized salt-templated carbon (OSTC) loaded iodine material. Meanwhile, the dual energy storage mechanism was revealed through *in situ* characterization and theoretical calculations: (1) in the double electron conversion mechanism (I_2/I^-), only one step redox reaction occurred; (2) OSTC surface is rich in C=O groups, which can react with Zn^{2+} to form C–O–Zn groups, providing additional pseudo capacity for SZIBs; (3) the synergistic effect of oxygen-containing functional groups and porous carbon inhibited the formation of polyiodide and avoided its shuttle effect.

2.2 Polymer hosts

Besides carbon-based materials, some polymers have also emerged as carrier materials for iodine species redox and they usually have stronger binding ability with polyiodides. The positively charged nitrogen sites (–NH–$^+$ and –NH=$^+$) in the polymer chain provide binding sites for iodine. For instance, polyaniline (PANI)[63] has been utilized as the host material for iodine, with high conductivity through the doping of polyiodides into the conjugated polymer backbones. Zeng *et al.*[63] reported a method of de-doping and re-doping to introduce iodine species into the polyaniline (PANI) framework. During the redox process, iodine was effectively immobilized within the backbone of PANI in the form of I_5^-, I_3^-, or I^- by coulombic force, thereby suppressing iodine sublimation during the manufacturing process and polyiodide dissolution during cycling. Consequently, an impressive reversible capacity of 160 mA h g^{-1} and remarkable cycling stability were achieved, with a notable capacity retention of 79% after 700 cycles at 1.5 A g^{-1}. Wu *et al.*[58] also used conductive PANI as a carrier for polyiodide, which contains positively charged nitrogen sites that effectively bind to polyiodide anions. At the same time, the complex can be adjusted in the $ZnCl_2$ electrolyte to eliminate free iodine anions and inhibit the further formation of polyiodides. Therefore, the optimized aqueous zinc-iodine battery exhibited excellent cycling performance and CE, achieving a capacity of 2 mA h cm^{-2} at 6 mA cm^{-2}, accompanied by a remarkable CE of 99.2%. Furthermore, it exhibited capacity retention of 99.9% after 1000 cycles (Fig. 4e). Moreover, in order to verify the stronger adsorption performance of PANI in conductive polymers, the structure and properties of PANI and PPy were analyzed.[64] The study revealed that microporous PANI exhibited a high specific surface area and porosity, thereby providing an abundance of active adsorption sites to effectively minimize the shuttling of polyiodide ions. However, the dense PPy significantly impedes electrolyte diffusion, induces the formation of non-conductive dense iodine films, and consequently leads to poor electrochemical performance.

During the exploration of polymer cathode materials, it was discovered that a cost-effective natural biopolymer material (starch) firmly anchors the polyiodide species. Unlike the aforementioned conductive polymer iodine doping strategy, the unique double helix structure of starch can be effectively confined within the helical chain through bonding, which has

a good capture ability for iodine species.[65] Zhang *et al.*[23] proposed a starch structure restriction strategy to enhance the constraint ability of polyiodine ions. As depicted in Fig. 5a, the DFT and *in situ* analysis confirmed that the dissolution of polyiodide was inhibited. The aqueous SZIBs exhibited excellent electrochemical performance, achieving a high coulombic efficiency of ≈100% and specific capacity of 182.5 mA h g^{-1} at 0.2 A g^{-1}, while a long cycle life of over 50 000 cycles at a high current density of 10 A g^{-1}. This research also lays the foundation for designing next-generation SZIBs without the shuttle effects.

Although these polymers have strong binding ability to iodine species, their electrical conductivity is very weak, which is the main shortcoming. How to overcome this has become a problem that needs further consideration.

2.3 Functional framework structure

In recent years, the metal–organic frameworks (MOFs) have emerged as promising precursors for the synthesis of heteroatom-doped porous carbon materials due to their unique advantages such as high specific surface area, tunable pore size, and adjustable structure.[41,42] For example, Prussian blue compounds have an open framework structure and three-dimensional ion channels, making them very suitable for rapid ion migration. Gao *et al.*[66] incorporated iodine ions into Prussian blue (PB) through the pre-embedding method, facilitating the formation of ferrum-iodine bonds that effectively reduced the electrochemical reaction energy barrier of subsequent iodine ions at the pre-embedding site. More importantly, the kinetic process of triiodide/iodide (I_3^-/I^-) redox was enhanced, and the self-shuttle of polyiodide was effectively inhibited. The PBI electrode maintained a CE of ≈100% over 3500 cycles, indicating that the self-shuttle effect was significantly suppressed.

However, the limited active sites of Prussian blue resulted in a low utilization rate of iodine. In order to enhance the utilization of iodine, Li *et al.*[67] reported a supermolecule mineralization strategy for constructing covalent organic frameworks (COFs), which primarily governed the synthesis of semiconductor COF nanostructures through pre-assembly and subsequent *in situ* covalent immobilization of supermolecules. The customized COF possessed a nanostructure and polar functional groups, exhibiting excellent iodine adsorption properties. As illustrated in Fig. 5b, the pyridine N-species within PY-2PBA functioned as active centers, facilitating the kinetics of the redox reaction of polyiodide while simultaneously immobilizing it. Additionally, the limitation of polar pyridine N-species and the electron delocalization polarization supply of polyiodide species in PY-2PBA nanostructures were the main reasons for its excellent performance. The SZIBs exhibited a high active iodine loading content of 80%, remarkable specific capacity (192.3 mA h g^{-1} at 0.5 A g^{-1}), and excellent long-term cycling stability (156 mA h g^{-1} at 2 A g^{-1} after 2800 cycles).

However, the current limitation lies in the low potential univalent state transition (I^-/I^0) of aqueous SZIBs, which hinders their further advancements in output voltage and energy density. This bottleneck also poses challenges for practical applications of current aqueous SZIBs. Zhi's group reported that the introduction of the main chain of $Ti_3C_2I_2$ MXene effectively enhanced electron conduction, confinement effects, and reaction kinetics.[68] Therefore, $Ti_3C_2I_2$ MXene is employed as the principal material for iodine. The effective suppression of the shuttle effect ensured that the battery exhibited excellent long-cycle performance and rate capability. Meanwhile, in comparison to conventional I^-/I^0 redox reactions, the presence of Cl^- in the electrolyte stimulated the four-electron ($I^-/I^0/I^+$) double conversion reaction, thereby increasing the voltage platform of the reaction to 1.65 V (*vs.* Zn^{2+}/Zn). The high capacity and energy density of SZIBs have been achieved, reaching a remarkable 207 mA h g^{-1} and 280 W h kg^{-1}, surpassing the upper limit reported for the zinc-iodine system. Obviously, the synergistic regulation of both the cathode and electrolyte represents a novel approach for achieving high potential and high energy density in aqueous SZIBs.

The design of novel cathode materials is anticipated to promote the advancement of SZIBs.[69,70] Wang *et al.*[69] designed an organic-inorganic $MXDA_2SnI_6$ ($MXDA^{2+}$ denotes protonated *m*-xylylenediamine cation) perovskite microcrystal as an iodine host material. The incorporation of long-chain organic matrix at the A site and Sn^{2+} cations at the B-site of 0D $MXDA_2SnI_6$ perovskite offered physical constraints as well as chemical interactions to restrict the dissolution of polyiodide anions. As

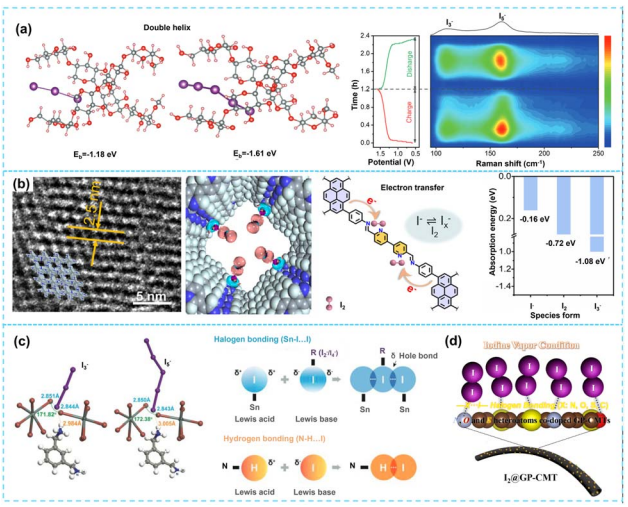

Fig. 5 (a) The optimized structure models of triiodides and pentaiodide ions interacting with the starch double helix, *in situ* Raman spectra showing the electrochemical process of I^-/I_2 conversion in starch-based SZIBs. Reproduced with permission.[23] Copyright 2022, Wiley-VCH. (b) TEM images of PY-2BPA COF, the optimized charge-density-difference patterns of I_2 adsorption on PY-2BPA COFs, and adsorption energy for I^-, I_2, and I_3^- on PY-2BPA COF. Reproduced with permission.[67] Copyright 2023, Elsevier. (c) Confinement of polyiodide ions in the 0D $MXDA_2SnI_6$ perovskite, coordination between perovskite lattice and I_3^- and I_5^- ions, and mechanisms of related intermolecular interactions. Reproduced with permission.[69] Copyright 2023, Wiley-VCH. (d) Schematic illustration of the halogen bond functionality on suppressing I^- losses. Reproduced with permission.[55] Copyright 2022, Elsevier.

shown in Fig. 5c, the DFT theoretical calculations demonstrated robust halogen combining between $MXDA_2SnI_6$ perovskite and polyiodide ions (I_3^- and I_5^-). This strong interaction made the I_5^- anion dominant at the end of the charging process, effectively alleviating the formation of triiodide ions. This research validates the feasibility of employing ion perovskite as conversion cathodes and propels advancements in cathode electrode materials for SZIBs. Lastly, for the construction of organic functional framework structures, there may be structural modifications or partial collapse caused by the thermal decomposition of organic precursors, and the working mechanism still needs further in-depth research.

2.4 Design of composite materials

The development of low-cost composite materials is crucial for the practical application of aqueous SZIBs. Compared to traditional carbon hosts, composite materials exhibit superior iodine species anchoring capabilities, which can prevent the unnecessary dissolution of polyiodide ions. The composite materials are interconnected through some kind of bond bridge, which can combine the advantages of materials, effectively enhance conductivity, and inhibit shuttle effects. Chai *et al.*[55] designed graphite/porous carbon microtubules (GP-CMTs) composites and enhanced the strong interaction between iodine and iodine host through the –I·Y– halogen bond (Y refers to O, S, N, *etc.*). As depicted in Fig. 5d, the strong interaction and porous characteristics of this framework facilitated the absorption/fixation of iodine substances while preventing dissolution/loss of I-based redox active materials during charging and discharging. The quasi-solid-state zinc-iodine system exhibited an impressive energy density of up to 182.5 W h kg^{-1} at 0.42 kW kg^{-1} and excellent cycle stability (89.3% capacity retention over 103 cycles). Zhang *et al.*[44] reported that the heterogeneous structure of graphene/polystyrene pyrrolidone (G/PVP) effectively suppressed the shuttle effect. On the one hand, the strong π–π interaction between G and PVP contributed to the uniform stability of the G/PVP structure.[32] On the other hand, PVP effectively inhibited the shuttle effect due to the strong electrostatic interaction between PVP and iodine species. The unique energy storage mechanism involving conversion reactions provided ample Zn^{2+} for the anode, resulting in significantly improved the energy density (162 W h kg^{-1}) and long-lasting cycle stability (63.8% capacity retention after 200 cycles). Simultaneously, the composite materials were formed by combining the metal–organic frameworks with polypropylene.[71] The MOFs precursors exhibited excellent structural stability and transformed into carbon materials with an ideal porous structure upon carbonization and effectively captured iodine within a confined space. It not only inhibited the loss of active substances but also ensured its high utilization and efficiency. Moreover, the double-layer cathode structure[72] and quaternization engineering strategy[72,73] were also reported. The double-layer cathode structure consists of a conductive layer (CL, used as a cathode current collector) and an inexpensive adsorption layer (AL, cathode extension). CL requires good conductivity, while AL requires strong adsorption capacity of the I_3^- ions. The quaternization engineering can realize solution-based iodine chemical conversion (I^-/I_3^-) by creating a large energy barrier between I_3^- and I_2, which prevent the production of solid I_2, thereby reducing the energy of iodine reaction pathway and resulting in a rapid cathode chemistry.

The quaternization strategy has high practicality, scalability, and also offers a novel approach for the design and development of large-scale, low-cost, and high-performance SZIBs.

In this review, the design and development of cathode materials for SZIBs in recent years are summarized (Table 1). Firstly, the porous carbon matrix is employed to physically adsorb iodine and inhibit the dissolution of its polyiodides. The adsorption behavior is determined by nanopore size and available surface area. However, the physical interaction between the porous carbon matrix and iodine is too weak to immobilize I_2 molecules or capture polyiodine anions over extended periods. These challenges can be addressed through heteroatom doping and the construction of oxygen-containing functional groups. Secondly, the polymer facilitates iodine loading through chemical adsorption. Because the polymer chain contains positively charged nitrogen sites (–NH=$^+$), it effectively provides a binding site for iodine. Additionally, the functional framework structure efficiently loads the iodine species through a combination of physical constraints and chemical interactions. This not only reduces the energy barriers for reactions but also facilitates swift reaction kinetics, ultimately leading to a high energy density. Nevertheless, the thermal decomposition of organic precursors results in structural alterations and partial collapses, highlighting the need for the additional optimization of structural properties. Ultimately, the resolution of multiple challenges encountered by SZIBs is achieved through the strategic utilization of the inherent advantages offered by composite materials. For the synergistic optimization of the cathode and electrolyte, the electrolyte rich in Cl^- ions will stimulate the four-electron ($I^-/I^0/I^+$) conversion reaction, achieving high potential and high energy density far beyond the upper limit of traditional SZIBs redox reaction (I_3^-/I^-). These findings lay down a solid foundation for advancing large-scale, cost-effective, high-performance, and practical application of SZIBs.

3. Zn anode

Zn metal stands out as a promising anode material due to its impressive theoretical capacity (820 mA h g^{-1} and 5855 mA h L^{-1}), low electrochemical potential (−0.76 V *vs.* the SHE), and abundant availability.[3] However, its practical utility is hindered by challenges such as dendrite formation, HER, corrosion, and passivation in aqueous electrolyte systems.[10] Notably, in SZIBs, Zn metal is particularly susceptible to severe corrosion caused by polyiodine ($Zn + I_3^- \rightarrow Zn^{2+} + 3I^-$), resulting in poor coulombic efficiency and limited cyclability. Therefore, safeguarding the Zn anode is a critical necessity.

Considering these harmful reactions starting from the electrolyte–anode interface, constructing isolation layers between them is a direct and effective way. Chen *et al.*[76] used a one-step

Table 1 Comparison of the electrochemical performances of SZIBs based on cathode modification

Cathode material	Iodine content in hosts	Discharge voltage	Discharge capacity	Cycle retention	Energy density	Ref.
I_2/NGA	60.8%	1.26 V	178 mA h g^{-1}	>1000 cycles@5C	—	48
HCNT-O	—	1.12 V	1932.3 μA h cm^{-2} (2 mA cm^{-2})	89.2% (after 2600 cycles)	1647.3 mW h cm^{-3}	57
I_2@C-50	49.9%	1.2 V	210 mA h g^{-1}	66% (after 10 000 cycles at 5 A g^{-1})	237 W h kg^{-1}	46
GC-PAN/I_2	40%	1.20 V	160.9 mA h g^{-1}	≈100% (over 17 000 cycles at 20C.)	59.5 W h kg^{-1}	73
$Ti_3C_2I_2$ MXene	—	1.65 V	207 mA h g^{-1}	80% (over 2800 cycles at 3 A g^{-1})	280 W h kg^{-1}	68
NCCs/I_2	50%	1.20 V	259 mA h g^{-1}	66% (over 3500 cycles at 5 A g^{-1})	282 W h kg^{-1}	35
I_2@NHPC	61.6%	1.24 V	219.3 mA h g^{-1} at 1.0C	≈100% (10 000 cycles at 5.0C)	72.6 W h kg^{-1}	36
I–BC_{HP}	42%	1.24 V	100 mA h g^{-1} (at 100 mA g^{-1})	60% (over 800 cycles at 300 mA h g^{-1})	—	39
C/I_2	40%	1.24 V	261.4 mA h g^{-1} at 1 A g^{-1}	88.1% (over 3500 cycles at 1 A g^{-1})	—	34
I_2-NPC	52%	1.37 V	345.3 mA h g^{-1} at 0.2C	80.9% (10 000 cycles at 10C)	—	37
CMK-3@I_2	60%	1.30 V	90 mA h g^{-1} at 5 A g^{-1}	80.6% (over 39 000 cycles at 10 A g^{-1})	150 W h kg^{-1}	47
G/PVP@ZnI_2	—	1.20 V	145.6 mA h g^{-1} at 0.2 A g^{-1}	80% (1000 cycles at 1 A g^{-1})	162 W h kg^{-1}	44
I_2@GP-CMTs	40.47%	1.42 V	266 mA h g^{-1} at 1.2 A g^{-1}	86.8% (after 103 cycles at 4 A g^{-1})	182.5 W h kg^{-1}	55
B-Fe-NC/I_2	30%	1.20 V	216 mA h g^{-1} at 1C	90% (300 cycles at 2C)	—	20
Starch	72.1%	1.20 V	182.5 mA h g^{-1} at 0.2 A g^{-1}	90.5% (50 000 cycles at 10 A g^{-1})	—	23
HOPG	—	1.20 V	277.7 mA h g^{-1} at 1 A g^{-1}	97.6% (15 000 cycles at 5 A g^{-1})	334.3 W h L^{-1}	59
I_2@NPCNFs-800	—	1.22 V	184.3 mA h g^{-1} at 0.5C	77% (10 000 cycles at 5C)	—	74
I_2@PY-2PBA/CNT	80%	1.25 V	156 mA h g^{-1} at 2 A g^{-1}	100% (2800 cycles at 2 A g^{-1})	320 W h kg^{-1}	67
I_2/OSTC	26.6%	1.22 V	185 mA h g^{-1} at 1 A g^{-1}	85.04% after 10 000 cycles at 1 A g^{-1}	—	62
PNC-1000-I_2	58%	1.22 V	175 mA h g^{-1} at 4 A g^{-1}	≈100% over 10 000 cycles at 0.2 A g^{-1}	320 W h kg^{-1}	52
rGO-I_2	71.69%	1.20 V	1 mA h cm^{-2} at 80 mA cm^{-2}	≈100% (2000 cycles at 50 mA cm^{-2})	—	60
rGO	—	1.20 V	257 mA h g^{-1} at 1 A g^{-1}	96.7% at 5 A g^{-1} over 2000 cycles	—	22
PANI-I_2	45%	1.18 V	230 mA h g^{-1} at 0.3 A g^{-1}	79% after 700 cycles at 1.5 A g^{-1}	—	63
0D $MXDA_2SnI_6$ perovskite	46%	1.25 V	206 mA h g^{-1} at 0.5 A g^{-1}	95% after 5700 cycles at 1 A g^{-1}	—	69
PBI	45%	1.25 V	197.2 mA h g^{-1} at 10 A g^{-1}	94% after 1500 cycles. at 4 A g^{-1}	142 W h kg^{-1}	66
I_2@APCC	57.4%	1.65 V	422 mA h g^{-1} at 2C	≈100% after 600 cycles at 0.5 A g^{-1}	117.6 W h kg^{-1}	50
PANI	—	1.18 V	2 mA h cm^{-2} at 6 mA cm^{-2}	99.9% after 1000 cycles at 6 mA cm^{-2}	—	58
Starch	35.5%	1.32 V	4.1 mA h cm^{-2} at 10 mA c m^{-2}	92% over 2000 cycles at 10 mA c m^{-2}	—	65
CNSs/I_2	33.8%	1.20 V	170.5 mA h g^{-1} at 100C	85% (6000 cycles at 100C)	219.5 W h kg^{-1}	38
PTCC900@I_2	40%	1.22 V	243 mA h g^{-1} at 0.5 A g^{-1}	≈100% after 50 000 cycles at 5 A g^{-1}	—	49
MOG-I	42%	1.35 V	184.9 mA h g^{-1} at 1C	95.1% (1500 cycles at 1C)	—	42
MPC/I_2	41%	1.20 V	137 mA h g^{-1} at 0.1 A g^{-1}	99.7% over 2000 cycles at 1 A g^{-1}	—	75
HCNS/$I_{0.5}$	—	1.25 V	295.7 mA h g^{-1} at 0.5 A g^{-1}	94%; 1500 cycles at 1 A g^{-1}	—	33
NiSAs-HPC/I_2	41.7%	1.20 V	141 mA h g^{-1} at 10C	93.4% after 10 000 cycles at 10C	—	56
I_2@C	70%	1.20 V	110.1 mA h g^{-1} at 12C	88.1% after 3000 cycles at 12C	—	32
I_2/Fe-CF-700-500	40%	1.00 V	214 mA h g^{-1} at 2C	≈100% after 5000 cycles at 5C	—	54
ZPC/I_2	25%	1.22 V	137 mA h g^{-1} at 800 mA g^{-1}	78%. after 1000 cycles at 800 mA g^{-1}	—	21

reaction to generate a phytic acid (PA) coating layer *in situ* on Zn anode. The PA can coordinate with Zn^{2+} to form a dynamic 3D molecular network, in which Zn^{2+} can migrate through a coordinated hopping mechanism, realizing a smooth Zn striping and plating process. Moreover, the PA layer can facilitate the desolvation process of Zn^{2+}, decreasing the amount of activated H_2O molecules, reaching the Zn metal surface and inhibiting the HER. Compared with such small organic molecules, polymers characterize higher molecular weight, exhibit greater continuity and flexibility, and are favorable for a denser coating formation. For examples, Yi *et al.*[77] proposed a cross-linked carboxymethyl chitosan-based gel coating on Zn anode, which provides a "flexible" substrate for zinc plating/stripping, leading to a flat real-time interface. Wang *et al.*[78] used renewable biomass-based lignin as an effective coating, which is rich in functional groups and a three-dimensional networked structure, suppressing the corrosion of I_3^- and H_2O. Recently, Zhang *et al.*[79] constructed a sulfonate-rich ion-exchange layer (SC-PSS) on Zn anode (Fig. 6a) to modulate the transport behavior of Zn^{2+} and the reaction chemistry of polyiodide at the anode-electrolyte interface. The massive sulfonic acid groups characterized with negative charges repulse the polyiodide and can bond with water molecules, diminishing the corrosion from polyiodide and water. Simultaneously, the SC-PPS layer can accelerate the Zn^{2+} transfer and restrict the rough diffusion, favorable for a homogeneous Zn deposition. As a result, the full

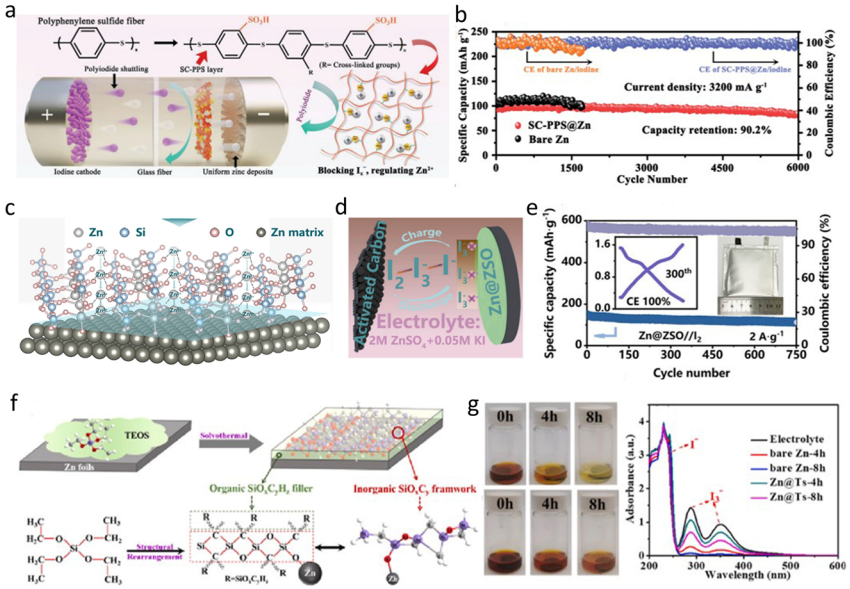

Fig. 6 (a) Schematic illustration of the SC-PPS synthesis process and its roles in realizing high-performance SZIBs. (b) Long-term cycling performance of SZIBs at 3.2 A g^{-1}. Reproduced with permission.[79] Copyright, 2023, Wiley-VCH. (c) The schematic illustration of the regulation mechanism of the Zn@ZSO anode. (d) The mechanism of iodide shuttling inhibition. (e) Cycling performance of pouch SZIB at 2 A g^{-1}. Reproduced with permission.[24] Copyright, 2022, Elsevier. (f) The formation mechanism of silicon-based composite coating on the Zn anode. (g) The visualized immersion tests of bare Zn (top) and Zn@Ts (bottom) in cathode and anode mixing electrolytes for different times and corresponding UV-vis spectra of electrolytes. Reproduced with permission.[80] Copyright, 2022, Elsevier.

battery using SC-PPS-coated Zn operated over 6000 cycles stably with 90.2% capacity retention and 99.89% average CE. By contrast, the battery with bare Zn only exhibited a short cycling of about 1700 cycles (Fig. 6b).

Besides organic coatings, inorganic coatings also performed well because of their higher mechanical strength. An in situ-formed disordered zinc silicate (ZSO) solid electrolyte interphase (SEI) with high Zn^{2+} conductivity of 9.29 mS cm^{-1} was designed by Peng *et al.*[24] to realize highly reversible Zn anode (Fig. 6c). The disordered ZSO interphase has sufficient tunnels for a fast transport of Zn^{2+} and redistribution of Zn^{2+} flux, guiding a uniform Zn deposition. Additionally, the ZSO interphase can inhibit I_3^- shuttling to the surface of Zn metal anode (Fig. 6d), well suppressing the self-discharge phenomenon of SZIBs. A pouch cell based on Zn@ZSO anode can operate up to 750 cycles at a current density of 2 A g^{-1} (Fig. 6e). Furthermore, Su *et al.*[80] prepared a kind of organic-inorganic composite silicon-based anticorrosion coating on Zn anode (Zn@Ts) *via* tetraethyl orthosilicate (TEOS) decomposition, forming a three-dimensional (3D) porous inorganic frameworks-SiO_xC_y, filled with organic polymers-$SiC_xO_yH_z$ (Fig. 6f). The 3D macroporous structure provides a strong mechanical framework and guides Zn^{2+} flux redistribution, realizing the uniform nucleation and deposition of Zn. In addition, the composite layer isolates the electrolyte and anode, which is beneficial to hindering the HER and corrosion. Fig. 6g shows that the color of electrolyte immersing bare Zn changed from brown to yellow, and the peak intensity of I_3^- ions in electrolyte decreased significantly in UV-vis spectra tests, demonstrating a corrosion reaction between I_3^- ions and Zn metal. By contrast, there was less color change of electrolyte soaking Zn@Ts, and the I_3^- signal only reduced slightly in UV-vis spectra, indicating a slow corrosion process of polyiodine to Zn metal due to the silicon-based coating. Benefiting from this, SZIBs achieved a specific capacity of 89 mA h g^{-1} and 93% capacity retention after 20 000 cycles.

At present, in the SZIBs system, the modification on the Zn anode is mainly to construct the coating. Despite the good results, this is not enough and there is still a large room for development. For example, the anode protection strategies in aqueous zinc ion batteries like three-dimensional framework design,[81] constructing desirable crystal planes,[82] and electrolyte additives[83,84] can also be cited. Other metal (like Li, Na) anode protection methods are also worth learning.

4. Modification of electrolytes

SZIBs are the leading technology for large-scale energy storage due to their inherent safety and low cost.[85,86] Electrolytes, as a crucial component of SZIBs, not only conduct solvated ions and regulate the solvation structure but also promote uniform SEI film formation on the zinc anode. We will next categorize electrolytes into liquid, solid, and eutectic types based on their physical state. Some work on upgrading zinc-iodine batteries based on electrolytes modification is summarized in Table 2.

4.1 Liquid electrolyte

Rechargeable aqueous zinc-iodine batteries, utilizing liquid water as the electrolyte solvent, are renowned for their affordability and exceptional safety features. However, there are still many challenges in their commercialization. On the Zn metal

Table 2 Comparison of the electrochemical performances of SZIBs based on electrolyte modification

Electrolyte	Discharge voltage	Discharge capacity	Cycle retention	Energy density	Ref.
4 M $ZnSO_4$ + 0.4 M LiI	1.16 V	0.42 mA h cm^{-2} (1 mA cm^{-2})	95% (after 5000 cycles)	211 W h kg^{-1}	87
2 M $Zn(CF_3SO_3)_2$	1.20 V	210 mA h g^{-1} (100 mA g^{-1})	66% (after 10 000 cycles)	237 W h kg^{-1}	46
2 M $Zn(CF_3SO_3)_2$ + 0.1 M ZnI_2	1.18 V	360.6 mA h g^{-1} (0.5C)	98.4% (after 35 000 cycles, at 50C)	422.6 W h kg^{-1}	88
1 M $ZnSO_4$ + vermiculite nanosheets	1.17 V	230.6 mA h g^{-1} (5C)	91.0% (after 13 000 cycles)		89
2M $ZnSO_4$ + pyridine	~1.23 V	105.5 mA h g^{-1} (10 A g^{-1})	~95% (after 25 000 cycles)		13
$ZnSO_4/ZnI_2$ in H_2O + EG	~1.17 V	388.8 mA h cm^{-3} (1 A g^{-1})	97.6% (after 15 000 cycles)	334.3 W h L^{-1} at 1.5 kW L^{-1} (based on cathode volume)	59
19 M $ZnCl_2$ + 19 M LiCl + 8 M ACN in H_2O	~1.61 V and 1.10 V	420 mA h g^{-1} (2000 mA g^{-1})	~82% (after 6000 cycles)	750 W h kg^{-1}	14
30 M $ZnCl_2$	~1.20 V, 1.60 V and 1.83 V	612.5 mA h $g_{I2}{}^{-1}$ (0.5 A $g_{I2}{}^{-1}$)	95.7% (after 2000 cycles, at 2 A g^{-1})	905 W h $kg_{I2}{}^{-1}$	90
20 M $ZnCl_2$ + 5 M KI	0.9 V	6.5 mA h cm^{-2} (2 mA cm^{-2})	100% (after 2000 cycles, at 50 mA cm^{-2})		60
Polymer gel matrix (F77, PEO53–PPO34–PEO53)	~1.28 V	210 mA h g^{-1} (1C)	94.3% (after 500 cycles)		91
Alginate-based polyanionic hydrogel	1.25 V	183.4 mA h g^{-1} (0.2 A g^{-1})	97.6% (after 200 cycles)		92
Acrylamide-based aqueous gel electrolyte	~1.75 V, 1.60 V and 1.25 V	1.91 mA h cm^{-2} (3 mA cm^{-2})	82% (after 500 cycles)		93
Iota-carrageenan (IC) gel electrolyte	~1.10 V	242 mA h g^{-1} (0.5C)	91.9% (after 5000 cycles, at 5C)		94
Eutectic electrolyte (*N*-methylacetamide)	1.12 V	2.19 mA h cm^{-2} (4 mA cm^{-2})	98.7% (after 5000 cycles)		45
Propylene glycol-based hydrated eutectic electrolyte	~1.20 V	195.7 mA h g^{-1} (5C)	97.9% (after 2000 cycles)		95
Sulfolane-based hybrid eutectic electrolyte	~1.1 V	164 mA h g^{-1} (105.5 mA g^{-1})	86% (after 2000 cycles)		96

side, the issue of inhomogeneous electric field distribution results in the growth of Zn dendrites during repeated plating/stripping processes, reducing the Zn utilization. Furthermore, the modulus of elasticity of Zn is approximately 20 times higher than that of Li, which suggests that undesired morphologies, such as non-planar deposition and metal orphans, can have consequences that are more severe compared to their lithium counterparts. Even worse, irreversible side reactions occur with by-products like zinc hydroxide and zincates during charging/discharging, potentially reducing the lifespan of the battery.[90,97] In addition, the occurrence of HER in the aqueous electrolyte accelerates the formation of layered double hydroxide (LDH) precipitation, forming a Zn^{2+} insulating layer. This interferes with the ion flux and further exacerbates the rapid growth of dendrites.[98,99] On the I_2 side, I^- reacts with I_2 *via* a strong halogen bond to form soluble triiodide (I_3^-). The trihalide then diffuses to oxidize the anode, leading to swift self-discharge.[100] In addressing the aforementioned challenges, a key emphasis lies in stabilizing the zinc metal anode and preventing polyiodide shuttling through deliberate electrolyte formulation design. Additionally, unraveling the solvation structure of the electrolyte has emerged as a focal point in research on SZIBs.

Adjusting Zn salt to alter the solvation structure in the electrolyte emerges as a potent method to stabilize zinc metal and suppress the shuttle of polyiodide. For example, Li and colleagues employed a 2 M $Zn(CF_3SO_3)_2$ electrolyte to safeguard the Zn anode and suppress the shuttling of triiodide ions. Through DFT calculations, it was discerned that the absolute binding energy value between $CF_3SO_3^-$ and I_2 is as low as 4.5 kcal mol^{-1}, suggesting promising coordination between free I_2 and $CF_3SO_3^-$ (Fig. 7a). This not only significantly bolstered the initial coulombic efficiency (enhanced from 61.1% to 91.3%) but also showcased high ionic conductivity and facilitated a robust SEI film formation on the Zn-metal surface. A zinc-iodine cell equipped with C-50 activated carbon boasted a commendable 66% capacity retention after 10 000 cycles at 5 A g^{-1}.[46] Although $Zn(CF_3SO_3)_2$ can well stabilize the Zn metal anode, the shuttle effect of I_3^- and I_5^- still persists in the electrolyte system, leading to low capacity retention in the battery. To address this, Chen *et al.* combined the use of layered porous carbon encapsulated iodine as the cathode material and the introduction of ZnI_2 to 2 M $Zn(CF_3SO_3)_2$ electrolyte, aiming to enhance polyiodide adsorption and reinforce the protection of the zinc metal anode. The incorporation of I^- ions effectively induces the growth of the Zn (002) crystal plane, enhancing the stability of the Zn anode interface.[88] Consequently, the

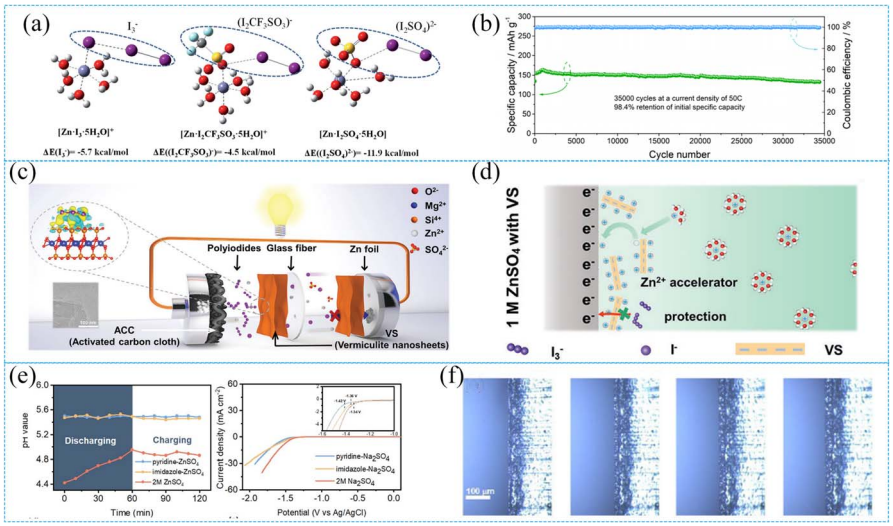

Fig. 7 (a) Potential pairing configurations within the electrolyte and density functional theory (DFT) calculations of binding energies. Reproduced with permission.[46] Copyright 2020, the Royal Society of Chemistry. (b) Cycling stability and CE at 50C after 35 000 cycles. Reproduced with permission.[88] Copyright 2021, American Chemical Society. (c) Schematic representation of SZIB in VS electrolyte. (d) Schematic diagrams of Zn anode shielded by a VS electrolyte. Reproduced with permission.[89] Copyright 2023, Wiley-VCH. (e) Real-time monitoring of pH values near the zinc anode and LSV curves of various electrolytes. Reproduced with permission.[102] Copyright 2023, Wiley-VCH. (f) *In situ* optical microscopy observations of Zn plating at 2 mA cm^{-2} at 0, 5, 10, and 15 minutes in pyridine-$ZnSO_4$. Reproduced with permission.[13] Copyright 2023, Wiley-VCH.

assembled zinc-iodine battery exhibits a capacity retention rate of 98.4% after 35 000 cycles at an elevated current density of 50C (Fig. 7b). Moreover, it achieves an ultra-high energy density of 422.6 W h kg^{-1} and a power density of 21.6 kW kg^{-1}. Additives have garnered considerable attention due to their ability to alter the solvation structure with just a minimal amount, which in turn influences the composition and structure of the SEI film on the zinc anode surface. This modification shifts the zinc deposition mode, leading to the formation of distinct crystallographic and surface structures.[101] For example, Chen and associates ingeniously fashioned a vermiculite nanosheet (VS) suspension electrolyte tailored to both confine polyiodide and stabilize zinc anodes (Fig. 7c). The high binding energy between polyiodide and the silica-oxygen bonds of VS ensures that the dissolved polyiodide is securely anchored to the surface of the VS suspended in the electrolyte. This smart design nips the shuttle effect in the bud. Moreover, the VS interfacial layer on the Zn anode keeps at bay side reactions triggered by polyiodides. The excess negative charge on the VS interlayer and surface gravitates toward Zn^{2+} ions from the diffusion layer, acting as an ionic catalyst for rapid Zn^{2+} transfer at the interface, ultimately ensuring a dendrite-free Zn plating/stripping behavior (Fig. 7d). Thanks to this strategy, the assembled zinc-iodine battery can be stably cycled 40 000 times at a rate of 20C.[89] Based on the repeated Zn plating/stripping processes accompanied by HER results in the periodical pH evolution at the Zn surface in AZIB, Zhang *et al.* proposed an interesting strategy for dynamic zinc interface regulation based on molecular switching. During galvanization, a rise in interfacial alkalinity instigated a molecular transition from GBL to γ-hydroxybutyrate (GHB). Concurrently, GHB robustly anchored itself to the Zn surface *via* triple Zn–O bonds, suppressing hydrogen evolution and fostering texture-conditioned Zn morphology. As Zn stripping occurred, fluctuating pH halted the molecular switching reaction, transitioning GHB back to GBL. This inventive molecular switching strategy attained impressive Zn reversibility with a 99.8% coulombic efficiency, and the zinc-iodine cell exhibited high cyclability, particularly at an elevated Zn depth discharge of 50%.[102] Similarly, to manage the periodic fluctuations of zinc surface pH, some additives can be used to mitigate changes. For instance, Lyu and his team introduced pyridine/imidazole to the electrolyte, thereby modulating the pH and preventing both HER and anodic corrosion (Fig. 7e and f). These compounds, by preferentially adhering to the Zn metal, orchestrate non-dendritic Zn plating/stripping. This culminates in a whopping coulombic efficiency of 99.6% and an extended cycling stability of 3200 h at 2 mA cm^{-2}, 2 mA h cm^{-2}. Pyridine, in particular, acts as a bulwark against polyiodide shuttling while promoting the I^-/I_2 conversion kinetics. Consequently, the zinc-iodine full cell flaunts cycle stability that exceeds a remarkable 25 000 cycles and a hefty specific capacity of 105.5 mA h g^{-1} at 10 A g^{-1}.[13]

Contrary to modifying the solute in the electrolyte, introducing organic solvents to alter the solvation structure has also yielded promising results. For instance, Zhang and his team demonstrated that by incorporating ethylene glycol (EG) into the aqueous electrolyte, one can effectively curtail polyiodide shuttling and unwanted side reactions on the Zn anode. This is attributed to the ability of EG to complex with polyiodide and modify the Zn^{2+} solvation structure. An SZIB that parades an enviable energy density of 334.3 W h L^{-1} at 1.5 kW L^{-1} and an awe-inspiring cycling stability spanning 15 000 cycles, retaining 97.6% capacity.[59]

Overall, the electrolyte additives can not only effectively form a stable SEI film on the Zn-metal interface, stabilize the Zn-metal negative electrode, reduce the HER, and retard the proliferation of Zn dendrites but also impede the shuttling effect of iodine species (I^-, I_3^-, and I_5^-), which can significantly prolong the cycling life of the Zn–I_2 battery. However, in the vast variety of additives, a complete selection criterion has not been established and is still in the experimental stage. In addition, the liquid electrolyte system has complexity and the interrelationships between additives and polyiodides, water molecules, Zn ions, and solvated Zn salt anions have not been proved experimentally in a good way, and further studies are needed.

The increased salt concentration effectively reduces the free water content, which has been proved to facilitate the uniform and stable deposition on Zn anode and suppress the HER.[103] For example, Chen *et al.* adopted an electrolyte modification strategy by incorporating high concentrations of $ZnSO_4$ (4 M) and LiI (0.4 M) as additives. The increased $ZnSO_4$ concentration facilitated the creation of more H_2O–H_2O hydrogen bonds in the high-concentration electrolyte, leading to a reduction in free H_2O molecules (Fig. 8a) and impeding the formation of $[Zn(H_2O)_6]^{2+}$, as well as curtailing H_2O-induced parasitic reactions such as zinc corrosion and hydrogen reduction. Moreover, iodide stabilized the zinc anode interface by inducing Zn(002) crystal growth, attributed to its optimal chemisorption on Zn(002) crystal surfaces (Fig. 8b). The competitive coordination of additional lithium ions and H_2O minimized by-product formation and ensured a smoother zinc deposition.[87] Compared to the zinc sulfate electrolyte, the modified electrolyte demonstrated ultra-long cycling stability, lasting 3000 hours at capacity of 1 mA h cm^{-2}, and featured low reversible deposition potentials around 40 mV. In addition to $ZnSO_4$, the more cost-effective $ZnCl_2$ also contributes to enhancing the stability of the Zn metal anode and inhibiting the shuttling of polyiodides. Ji *et al.* introduced a water-in-salt (WIS) electrolyte comprising 5 M KI and 15 M $ZnCl_2$. In this mixture, iodide is incorporated within the $[ZnI_x(OH_2)_{4-x}]_{2-x}$ complex (shown in Fig. 8c). This structure not only virtually eliminates the free iodide anion (9.25×10^{-3} M) but also impedes its potential reaction with I_2 to produce polyiodide.[100] After 300 cycles at a current density of 300 μA cm^{-2}, the capacity rose to as high as 4.1 mA h cm^{-2}, and the potential remained nearly constant through 500 cycles. Although some progress has been made with highly concentrated electrolytes, the high energy density of Zn metal anodes has not been fully utilized due to the fact that only one electron can be transferred per halogen ion. Therefore, Zou *et al.* unveiled a four-electron transfer aqueous zinc-iodine battery. This design effectively doubles the capacity of traditional iodine batteries by integrating a highly reversible I_2/I^+ pair alongside the conventional I^-/I_2 pair (Fig. 8d). Intriguingly, in the presence of strong solvation by the aqueous electrolyte, I^+ and Cl^- ions react to form ICl inter-halogens, which inhibits their hydrolysis. With respect to the iodine mass, the energy density of the battery reached an impressive value of 750 W h kg^{-1} (or 495 W h kg^{-1} considering the combined active mass of both positive and negative electrodes) (Fig. 8e and f). Furthermore, this design achieved an ultra-long cycling durability of 6000 cycles with a minuscule capacity decay rate of 0.003% per cycle at 2000 mA g^{-1}.[14] Liang *et al.* further developed this concept by achieving two redox centers, Cl and I, allowing for three-electron transfer with the use of 30 M $ZnCl_2$. In this system, during discharge, the cathodic iodine reacts with chloride ions of the electrolyte, inducing an interhalogen coordination chemical reaction that results in ICl_3^-. This innovative mechanism facilitates the reversible three-electron transfer reactions in redox-active halogen atoms (Fig. 8g–i). When tested in a laboratory-scale battery, this translated into an initial specific discharge capacity of 612.5 mA h $g_{(iodine)}^{-1}$, equivalent to a projected specific energy of 905 W h $kg_{(iodine)}^{-1}$.[90]

In conclusion, reducing the free water molecules in high-concentration electrolytes is advantageous for suppressing side reactions at the Zn anode and mitigating polyiodide shuttling, leading to elevated CE and increased specific capacity. Although WIS electrolytes have achieved significant milestones, the high salt content can increase the viscosity, escalate costs, and particularly, a high concentration of Cl^- salts may induce corrosion in the battery device, thereby hindering its practical applications. Consequently, the precise regulation of the composition and concentration of the electrolyte is critical to attain high CE, enhanced rate performance, and superior cycling stability in SZIBs.

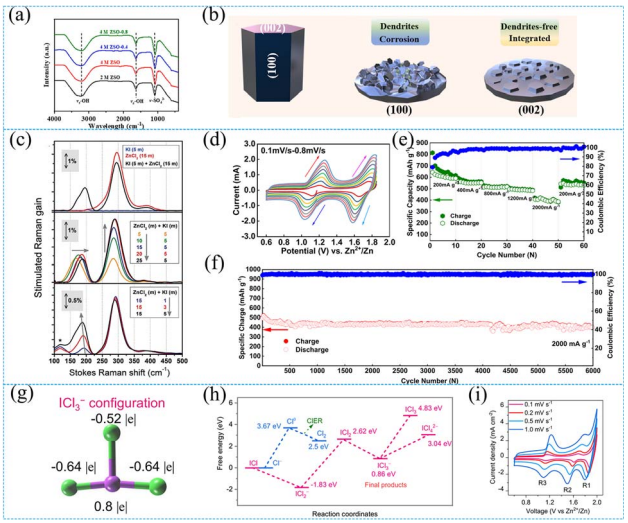

Fig. 8 (a) The crystal structure of metal Zn with (001) and (002) crystal planes. (b) The ATR-FTIR curves of different electrolytes. Reproduced with permission.[87] Copyright 2023, Elsevier. (c) Stimulated Raman spectroscopy analyses for varying concentrations of the WIS electrolytes Reproduced with permission.[100] Copyright 2023, Wiley-VCH. (d) CV curves obtained at various scanning rates from 0.1 mV s^{-1} to 0.8 mV s^{-1}. (e) Rate test at different current densities. (f) Long-term cycling at 2000 mA g^{-1} for 6000 cycles. Reproduced with permission.[14] Copyright 2023, Nature Publishing Group. (g) Energy profiles for potential reaction pathways and their respective corresponding products. (h) Configuration structure and valence states (atomic Mullikan charge) of ICl_3^- as the end product. (i) CV profiles of the Zn||Cl-I pouch cell. Reproduced with permission.[90] Copyright, 2023, Nature Publishing Group.

4.2 Gel electrolytes

In addition to liquid electrolytes, gel electrolytes, particularly hydrogels, have been gaining prominence in SZIB in recent years. Hydrogels play a crucial role in preventing I_3^- shuttling through their negatively charged polyanion chains. Moreover, they demonstrate a cation exchange capacity. Most importantly, hydrogels significantly improve the cycling durability of the zinc anode by addressing concerns such as zinc dendrite growth and corrosion reactions. Consequently, hydrogels have been the subject of extensive study as a promising electrolyte for SZIBs.[88,91,92,104] Sonigara *et al.* introduced the concept of solid-state AZIB with self-discharge control achieved by restricting iodide diffusion through solid–gel reactions. This approach utilizes a water-based gel, embedded with I_3^-/I^-, within a block copolymer containing highly active iodine components. This anionic gel is amphiphilic, ensuring both high solubility for iodine and ionic conductivity stemming from cubic microcrystalline self-assembled structures. The gel impedes the long-distance diffusion of iodine ions throughout the gel electrolyte layer, adhering to the multilayered self-assembled anion. Conversely, zinc ions diffuse with ease *via* the hydrophilic polyethylene oxide-rich channels (Fig. 9a and b). The resulting battery boasts a discharge capacity of 210 mA h g^{-1} at a rate of 1C (Fig. 9c) and showcases a robust stability, with 94.3% capacity retention after 500 cycles.[91] To further improve the electrochemical performance, double halogen conversion chemistry can be achieved by activating successive redox reactions of the halogen elements. For instance, Lv *et al.* prepared a quasi-solid-state zinc-double halide aqueous battery consisting of a suspended carbon cloth iodine cathode and an *in situ* prepared by concentrated gel hydroelectrolyte. The suspended composite cathode and the hydrogel electrolyte provided an iodine source and bromine ions, respectively, which activated the $I^-/I^0/I^+$ reaction to produce $[IBr_2]^-$ interhalogenin. The catalytic effect of iodine promotes the conversion reaction of Br^-/Br^0 in $[IBr_2]^-$ halides. Thus, this rationally designed double-halogen conversion chemistry enables three consecutive redox reactions (*i.e.*, I^-/I^0, I^0/I^+, and Br^-/Br^0). In addition, the $LiNO_3$ additive and acrylamide (AM)-based polymer matrix not only stabilized the anode/electrolyte interface but also inhibited side reactions and dissolution/diffusion of active substances. As a result, the assembled aqueous zinc double halide batteries exhibited high area capacity and energy density (Fig. 9d–f).[93] Contrary to employing double-halogen conversion chemistry to boost the electrochemical capacity, the formation of heterogeneous cells by introducing other reactions is also an effective approach. Liu *et al.* engineered dual network-structured hydrogel electrolytes by integrating polyacrylamide (PAM), sodium alginate (SA), and potassium iodide (KI) for solid-state zinc-air/iodide hybrid batteries. This ionic crosslinked dual network structure bestows the material with enhanced water absorption and retention (Fig. 9g) as well as superior mechanical strength and heightened ionic conductivity (Fig. 9h). Crucially, the incorporation of iodine species results in more favorable cathodic kinetics for iodide/iodate redox than oxygen electrocatalysis. This also adjusts the solvation structure of zinc ions, guaranteeing optimal interfacial stability. The finalized hybrid battery demonstrates

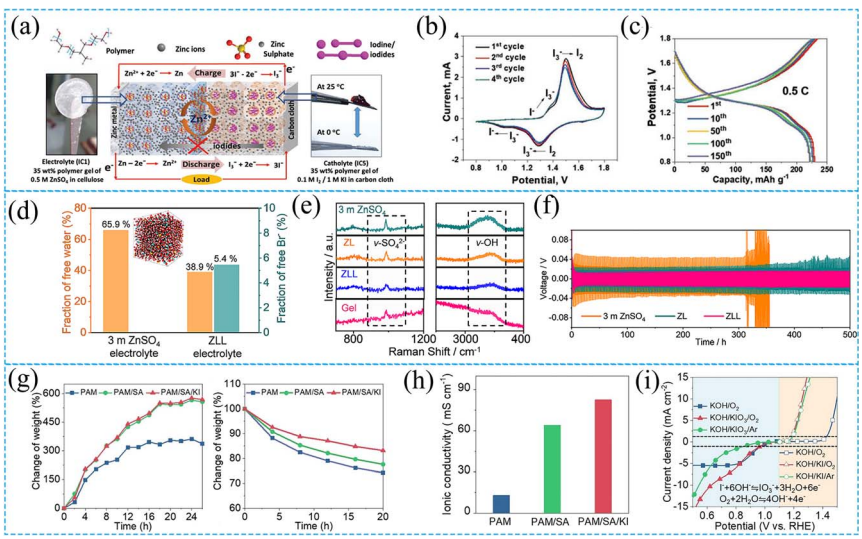

Fig. 9 (a) Schematic illustration of SZIBs operational mechanism featuring iodide diffusion control, with the chemical structures of component used in the battery at the top, a digital image of electrolyte IC1 embedded in cellulose on the left, and a digital image of the IC5 catholyte at room temperature and homogenized in carbon cloth at 0 °C on the right. (b) CV of SZIBs at 0.5 mV s^{-1}. (c) Galvanostatic charge/discharge of SZIBs at 0.5C. Reproduced with permission.[91] Copyright 2020, Wiley-VCH. (d) Summary of free water and Br^- content based on MD simulation. (inset) Snapshot of MD simulation for the ZLL electrolyte. The color code for the snapshot is as follows: red for O; white for H; yellow for S; gray for n; cyan for Br; pink for Li; blue for N. (e) Raman spectra comparing aqueous and gel electrolytes. (f) The cycling stability of Zn||Zn symmetric cells in various electrolytes at 0.5 mA cm^{-2} and sweep duration of 0.5 h. Reproduced with permission.[93] Copyright 2023, American Chemical Society. (g) Liquid electrolyte wettability and water retention capability, (h) ionic conductivity; (i) LSV curves of Pt/C + RuO_2 composites in different O_2 or Ar-saturated electrolytes at 5 mV s^{-1}. Reproduced with permission.[104] Copyright 2022, Wiley-VCH.

outstanding renewability and durable cycle life, lasting 110 hours and achieving energy efficiency of up to 80% (Fig. 9i).[104]

In general, gel electrolytes are effective at protecting the zinc anode and inhibiting polyiodide shuttling, while also providing flexibility. However, their complex preparation process, elevated manufacturing costs, and the associated decrease in battery energy density somewhat limit their broader application. Introducing alternative reactions into the system may improve the energy density, but this enhancement has been confined to the level of button batteries in laboratory settings and lacks scale-up validation, necessitating further comprehensive research.

4.3 Eutectic electrolytes

Deep eutectic solvents, which are eutectic mixtures of Lewis/Brownsted acidic anions and basic cations, stand out as novel ionic liquids that exhibit thermal stability at room temperature. When used as electrolytes in zinc-based batteries, the substitution of a non-aqueous solvent for water within the Zn^{2+} dissolution structure, which diminishes water activity and thereby enhances the stability of the zinc anode plating/stripping process.[105,106] However, they also exhibited notable limitations, such as poor Zn^{2+} diffusion efficiency, attributed to low electron conductivity and elevated viscosity.[107] Addressing these challenges, Yang *et al.* conceived an *n*-methylacetamide-based eutectic electrolyte for zinc-iodine batteries. This design incorporates a denser inner layer of I^- and CF_3SO_3, complemented by an outer layer of H_2O and C_3H_7NO. By judiciously controlling the quantity of free H_2O, they weakened the electrostatic interactions of I^- (an active substance) with adjacent ions (molecules), effectively inhibiting the formation of I_3^- during the I_2 reduction process (Fig. 10a and b). The zinc-iodine battery, integrated with an activated carbon-coated carbon fiber cloth, delivered an impressive capacity retention of 98.7% after 5000 cycles at 4.0 mA cm^{-2} and a near-perfect single-cycle coulombic efficiency.[45] The water in the Zn^{2+} solvated structure is replaced by a non-aqueous solvent, leading to reduced water activity, which can significantly enhance the cyclic stability of Zn metal. Unfortunately, partially hydrated Zn^{2+} solvated sheaths experience greater desolvation losses compared to fully hydrated Zn^{2+} solvated sheaths. This difference can result in slow interfacial charge transfer and high zinc deposition overpotentials. In response to this challenge, Li *et al.* developed a cost-effective and non-flammable sulfolane-based hybrid eutectic electrolyte to mitigate these side reactions. This development facilitated dendrite-free Zn coating/stripping, largely owing to the strong hydrogen bonding network of sulfolane-water. This not only lowers the water activity but also ensures a fully hydrated Zn^{2+} solvated structure, promoting rapid interfacial charge transfer. Remarkably, the average coulombic efficiency of the Zn–Cu cell reaches as high as 99.8% at a commercially relevant equivalent capacity of 4 mA h cm^{-2} (Fig. 10c). Furthermore, the Zn–Zn can be cyclically stabilized for 1600 hours at 8 mA h cm^{-2} (Fig. 10d). Additionally, the assembled utility-grade soft-pack cells offer an area capacity of 2.8 mA h cm^{-2}, maintaining 88% capacity retention after 300 cycles at 0.2C (Fig. 10e).[96] Although eutectic electrolytes can

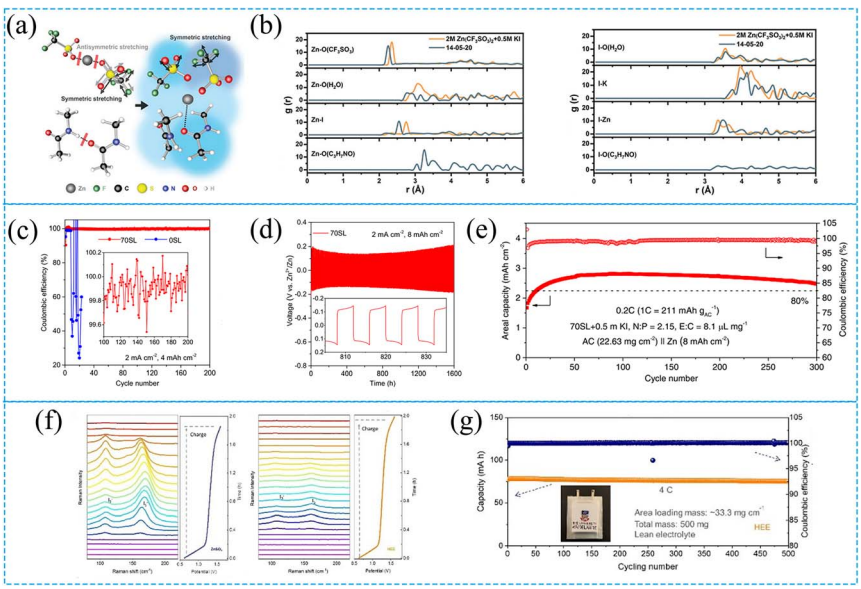

Fig. 10 (a) Schematic representation of eutectic solution formation mechanism with varying $Zn(CF_3SO_3)_2$/N-ACE molar ratios from 1 : 2 to 1 : 8. (b) Calculated radial distribution functions (RDFs) for Zn^{2+} and I^- from MD simulations in 2 M $Zn(CF_3SO_3)_2$ + 0.5 M KI and 14-05-20 solutions, respectively. Reproduced with permission.[45] Copyright 2022, the Royal Society of Chemistry. (c) CE of Zn||Cu batteries at 2 mA cm^{-2} with a capacity of 4 mA h cm^{-2}. (d) Galvanostatic Zn stripping/plating observed in Zn||Zn symmetric batteries with 70SL at 2 mA cm^{-2} with a capacity of 8 mA h cm^{-2}. € Long-term cycling performance of high-loading AC in 70SL + 0.5 m KI at 0.2C with a controlled N/P ratio of 2.15. Reproduced with permission.[96] Copyright 2023, Nature Publishing Group. (f) *In situ* Raman spectroscopy used to monitor the changes on the electrode surface in aqueous $ZnSO_4$ or HEE. (g) Cycling longevity of Zn–I_2 pouch cell tested at 4C, with the inset depicting the pouch cell designed for high mass loading of 33.3 mg cm^{-1}. Reproduced with permission.[95] Copyright 2023, Wiley-VCH.

effectively improve the reversibility of zinc, the zinc salts commonly utilized, such as $Zn(CF_3SO_3)_2$ and $Zn(TFSI)_2$,[108] are costly, while those based on $ZnCl_2$ are highly corrosive.[109,110] In light of this, Hao recently introduced a novel $ZnSO_4$-propylene glycol-based eutectic electrolyte. This electrolyte boosts exceptional fire resistance and an impressively low cost, amounting to less than 1/200 of $ZnCl_2/Zn(CF_3SO_3)_2/Zn(TFSI)_2$. Importantly, it effectively inhibits the I_2 shuttle effect and minimizes side reactions at the Zn anode (Fig. 10f). Consequently, during 1C cycling of the button SZIB, the electrolyte demonstrated exceptional cycling performance, retaining 91.4% capacity even at 20C. When incorporated into the pouch cell, a record mass loading of 33.3 mg cm^{-2} was achieved, with the capacity after 500 cycles remaining at an impressive 96.7% (Fig. 10g), outperforming other solution cells.[95]

The hydrogel electrolytes and eutectic electrolytes have demonstrated their ability to proficiently modulate zinc ion deposition. Furthermore, the coordination effect of their anions with iodine effectively prevents polyiodide shuttling. This makes them promising candidates for zinc-iodide batteries that prioritize long cycle life and enhanced safety. Despite these advances, understanding the reaction mechanism of iodide in zinc-iodide batteries remains a challenge. Additionally, the employment of gel or high-concentration electrolytes can elevate fabrication costs and diminish the energy density of the batteries, potentially hampering their scalability and broader adoption. To address these challenges, it is crucial to further design electrolyte compositions. The future development of electrolytes should center around two primary objectives: (1) ensuring compatibility with iodine substances on the cathode side while maintaining reversible Zn metal plating/stripping on the anode side. (2) Equipping them with the capability to curb polyiodide migration is a fundamental necessity for achieving prolonged battery cycle life.

5. Separators design

Currently, glass fiber (GF) separators are predominantly employed as separators in SZIBs. However, these fiber separators lack the capability to effectively regulate ion transmission, leading to the potential formation of a concentration gradient near the Zn anode. Moreover, their relatively wide pores facilitate the unhindered passage of polyiodine ions. Therefore, it is crucial to develop novel strategies to enhance the performance of general GF separators or new separators. One straightforward approach involves the surface modification of the separator with other substances to attain the desired functionality. For example, Hou *et al.*[75] developed a single-sided separator using Ketjen Black-modified cotton fibers (KB@CF), which enhanced the electronic conductivity and effectively anchored iodine species. When combined with a mesoporous carbon cathode host derived from metal–organic frameworks (MOF), the zinc-iodine battery demonstrated impressive electrochemical performance. Specifically, at a current density of 0.1 A g^{-1}, the battery equipped with the KB@CF separator maintained a specific capacity of 137 mA h g^{-1} after 300 cycles, whereas the

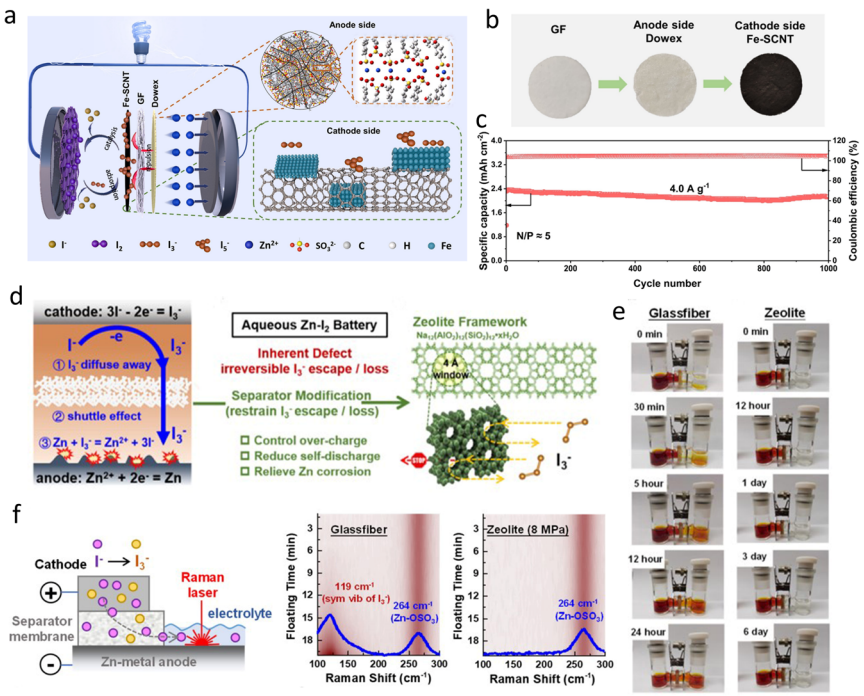

Fig. 11 (a) Schematic diagram of the Dowex + Fe-SCNT/GF separator mechanism. (b) Optical photos of Dowex + Fe-SCNT/GF separator. (c) Cycling performance of SZIBs with the Janus separator at 4.0 A g^{-1}. Reproduced with permission.[53] Copyright 2023, Wiley-VCH. (d) Schematic illustration of SZIBs critical problems and the zeolite molecular sieve working mechanism. (e) Penetration test with glass fiber separator (left) and zeolite membrane (right). (f) *In situ* Raman spectroscopy technology to observe the shuttle of I_3^- diffusion. Reproduced with permission.[111] Copyright 2022, American Chemical Society.

battery with a CF separator only retained 75 mA h g^{-1}. Inadequately, Ketjen Black (KB) merely imposes a physical constraint on iodine species and lacks the capacity to expedite their transformation. Iron (Fe), on the other hand, has demonstrated strong chemical interactions with iodine species and is frequently employed in SZIBs. Kang *et al.*[53] introduced a Janus separator to concurrently enhance the stability of cathode/anode interfaces (see Fig. 11a). One side of the Janus separator featured Fe nanoparticle-decorated single-wall carbon nanotubes (Fe-SCNT), which is facing the cathode, while the other side was coated with cation exchange resin Dowex for the anode protection (see Fig. 11b). The Fe-SCNT effectively anchored polyiodides and catalyzed their redox kinetics, while the Dowex contained abundant $-SO_3^-$ groups that attracted Zn^{2+} ions and repelled SO_4^{2-} ions and polyiodides. Consequently, this Janus separator conferred exceptional performance to SZIBs, achieving a high reversible areal capacity of 2.4 mA h cm^{-2} for over 1000 cycles at 4.0 A g^{-1} (see Fig. 11c).

Modifying the separator surface has to be proven effective to some extent; it is important to note that fiber separators possess relatively large pores that cannot be entirely blocked by the modification layer. Consequently, polyiodine may still migrate from one side of the separator to the other after long time cycling. Given this limitation, there is an urgent need to explore alternative functional separator materials. Zhou's research team[41,111] has focused on restraining iodine species using the angstrom-sized pores of metal–organic frameworks (MOF) or zeolites, yielding promising outcomes. For instance, they employed a compact and flexible zeolite molecular sieve membrane with precisely ordered framework windows to inhibit I_3^- crossover (see Fig. 11d). The porous framework of zeolite features 4 Å windows, smaller than the soluble I_3^- ions (5.14 Å), effectively trapping I_3^- within the catholyte region. This was demonstrated in visual penetration experiments (see Fig. 11e), where the shuttle phenomenon occurred from the outset in the H-type cell using a glass fiber separator, whereas no polyiodine shuttle was observed even after 6 days of use with the zeolite membrane. *In situ* Raman spectra further supported its ability to restrain iodine species (see Fig. 11f).

The signal of I_3^- at 119 cm^{-1} was clearly detected in the glass-fiber-based *in situ* cell, while no I_3^- signal was observed in the zeolite-based *in situ* cell. Comparatively, when using the zeolite membrane separator, the coulombic efficiency of the SZIBs improved significantly, from 78.9% to 98.6% at 0.2 A g^{-1}, compared to batteries with glass fiber separators. However, it is worth noting that due to its small aperture, the mass transfer process will slow down accordingly, which will sacrifice other performance of the battery to some extent. Therefore, the development of more new functional separators is necessary and related research is rare at the current stage, which may be a new avenue waiting to be developed.

6. Summary and prospects

Aqueous zinc-iodine batteries demonstrate strong competitiveness in energy storage devices owing to their high safety, low cost, and eco-friendly characteristics. Nevertheless, certain intrinsic drawbacks in this system, such as the "shuttle effect", sluggish kinetics, zinc dendrites, and side reactions, impede its development. To conquer these problems, researchers have exerted significant efforts and continue to make breakthroughs. In this review, we elucidate the advantages of SZIBs, outline their operational mechanisms, and delve into the primary challenges they encounter. The research status of key components such as the cathodes, anodes, electrolytes, and separators are meticulously analyzed and summarized.

Despite the fruitful advances, research on static zinc-iodine batteries is still in its early stages. More focused efforts are needed to deepen our understanding of this system and develop more applicable strategies. In the meantime, the following questions are worth referring to. (1) Regarding the cathode, there is potential in designing porous carbon materials with a limited structure, given their lightweight nature and excellent electrical conductivity. However, there is a need for further optimization to enhance their interaction with iodine species. Additionally, it is crucial to explore methods that are suitable for mass production as the current synthesis predominantly occurs in small laboratory quantities and involves a complex process. (2) Concerning the anode, a viable improvement strategy can be drawn from the anode protection methods employed in aqueous zinc-ion batteries, leveraging the wealth of related research in this area. However, it is essential to consider the impact of polyiodide ions, assessing factors such as the resistance of the coating to polyiodide ion corrosion. (3) There is an urgent need to develop functional separators that can effectively block polyiodide without compromising other battery performance aspects. (4) Cathode binders play a crucial role in static zinc-iodine batteries despite not being highlighted earlier. Currently, the primary binders employed are PVDF and PTFE. However, both are hydrophobic, which hampers interfacial infiltration and mass transfer. Moreover, during the preparation process, a portion of I_2 is lost due to the solvent used, such as N-methylpyrrolidone (NMP), which exhibits good solubility toward I_2.

In conclusion, static zinc-iodine batteries hold promising prospects, provided there are concerted efforts to explore their potential. We believe that this review will offer valuable reference and guidance for ongoing research on static zinc-iodine batteries.

Data availability

The type of this manuscript is a review and related data are cited from others. Therefore, there are no raw experimental or computational data associated with this article.

Author contributions

Z. Bai, G. Wang, H. Liu, and Y. Lou contributed equally to this work. Z. Bai designed the structure of the review. G. Wang, H. Liu, and Y. Lou collected the papers related to this review topic and co-wrote the paper. The manuscript was revised by all the authors.

Conflicts of interest

There are no conflicts to declare.

Acknowledgements

Z. B. thanks the financial support of National Natural Science Foundation of China (No. 22272093) and Natural Science Foundation of Shandong Province (ZR2021MB127). N. W. acknowledge support from the Australian Research Council (ARC) (DE200101384, DP240102926, and LP180100722) and a 2021 RevlTAlising research grant from the University of Wollongong.

References

1 G. Zhou, L. Xu, G. Hu, L. Mai and Y. Cui, Nanowires for Electrochemical Energy Storage, *Chem. Rev.*, 2019, **119**, 11042–11109.
2 Y. Wang, R. Wang, K. Tanaka, P. Ciais, J. Penuelas, Y. Balkanski, J. Sardans, D. Hauglustaine, W. Liu, X. Xing, J. Li, S. Xu, Y. Xiong, R. Yang, J. Cao, J. Chen, L. Wang, X. Tang and R. Zhang, Accelerating the energy transition towards photovoltaic and wind in China, *Nature*, 2023, **619**, 761–767.
3 C. Nie, G. Wang, D. Wang, M. Wang, X. Gao, Z. Bai, N. Wang, J. Yang, Z. Xing and S. Dou, Recent Progress on Zn Anodes for Advanced Aqueous Zinc-Ion Batteries, *Adv. Energy Mater.*, 2023, **13**, 2300606.
4 C. Li, S. Cong, Z. Tian, Y. Song, L. Yu, C. Lu, Y. Shao, J. Li, G. Zou, M. H. Rümmeli, S. Dou, J. Sun and Z. Liu, Flexible perovskite solar cell-driven photo-rechargeable lithium-ion capacitor for self-powered wearable strain sensors, *Nano Energy*, 2019, **60**, 247–256.
5 F. Niu, Z. Bai, Y. Mao, S. Zhang, H. Yan, X. Xu, J. Chen and N. Wang, Rational design of MWCNTs@amorphous carbon@MoS_2: Towards high performance cathode for aqueous zinc-ion batteries, *Chem. Eng. J.*, 2023, **453**, 139933.
6 X. Gu, J. Wang, X. Zhao, X. Jin, Y. Jiang, P. Dai, N. Wang, Z. Bai, M. Zhang and M. Wu, Engineered nitrogen doping on VO_2(B) enables fast and reversible zinc-ion storage capability for aqueous zinc-ion batteries, *J. Energy Chem.*, 2023, **85**, 30–38.
7 Y. Zong, H. He, Y. Wang, M. Wu, X. Ren, Z. Bai, N. Wang, X. Ning and S. X. Dou, Functionalized Separator Strategies toward Advanced Aqueous Zinc-Ion Batteries, *Adv. Energy Mater.*, 2023, **13**, 2300403.
8 F. Wu, F. Du, P. Ruan, G. Cai, Y. Chen, X. Yin, L. Ma, R. Yin, W. Shi, W. Liu, J. Zhou and X. Cao, Regulating zinc deposition behaviors by using a functional PANI modification layer on a separator for high performance aqueous zinc-ion batteries, *J. Mater. Chem. A*, 2023, **11**, 11254–11263.
9 D. Wang, H. Liu, D. Lv, C. Wang, J. Yang and Y. Qian, Rational Screening of Artificial Solid Electrolyte Interphases on Zn for Ultrahigh-Rate and Long-Life Aqueous Batteries, *Adv. Mater.*, 2023, **35**, 2207908.
10 C. Wang, D. Wang, D. Lv, H. Peng, X. Song, J. Yang and Y. Qian, Interface Engineering by Hydrophilic and Zincophilic Aluminum Hydroxide Fluoride for Anode-Free Zinc Metal Batteries at Low Temperature, *Adv. Energy Mater.*, 2023, **13**, 2204388.
11 J. Han, Z. Chen, J. Xu and J. Han, A novel electrolyte study on polyaniline aqueous zinc-ion battery, *Mater. Lett.*, 2021, **304**, 130629.
12 W. Wu, S. Wang, L. Lin, H.-Y. Shi and X. Sun, A dual-mediator for a sulfur cathode approaching theoretical capacity with low overpotential in aqueous Zn–S batteries, *Energy Environ. Sci.*, 2023, **16**, 4326–4333.
13 Y. Lyu, J. A. Yuwono, P. Wang, Y. Wang, F. Yang, S. Liu, S. Zhang, B. Wang, K. Davey, J. Mao and Z. Guo, Organic pH Buffer for Dendrite-Free and Shuttle-Free Zn-I_2 Batteries, *Angew. Chem., Int. Ed.*, 2023, **62**, e202303011.
14 Y. Zou, T. Liu, Q. Du, Y. Li, H. Yi, X. Zhou, Z. Li, L. Gao, L. Zhang and X. Liang, A four-electron Zn-I_2 aqueous battery enabled by reversible $I^-/I_2/I^+$ conversion, *Nat. Commun.*, 2021, **12**, 170.
15 W. Ma, T. Liu, C. Xu, C. Lei, P. Jiang, X. He and X. Liang, A twelve-electron conversion iodine cathode enabled by interhalogen chemistry in aqueous solution, *Nat. Commun.*, 2023, **14**, 5508.
16 Z. Zhang, Y. Zhu, M. Yu, Y. Jiao and Y. Huang, Development of long lifespan high-energy aqueous organic||iodine rechargeable batteries, *Nat. Commun.*, 2022, **13**, 6489.
17 D. Lin and Y. Li, Recent Advances of Aqueous Rechargeable Zinc-Iodine Batteries: Challenges, Solutions, and Prospects, *Adv. Mater.*, 2022, **34**, 2108856.
18 C. Bai, F. Cai, L. Wang, S. Guo, X. Liu and Z. Yuan, A sustainable aqueous Zn-I_2 battery, *Nano Res.*, 2018, **11**, 3548–3554.
19 K. Lu, H. Zhang, B. Song, W. Pan, H. Ma and J. Zhang, Sulfur and nitrogen enriched graphene foam scaffolds for aqueous rechargeable zinc-iodine battery, *Electrochim. Acta*, 2019, **296**, 755–761.
20 M. Liu, Q. Chen, X. Cao, D. Tan, J. Ma and J. Zhang, Physicochemical Confinement Effect Enables High-Performing Zinc–Iodine Batteries, *J. Am. Chem. Soc.*, 2022, **144**, 21683–21691.
21 J. Xu, J. Wang, L. Ge, J. Sun, W. Ma, M. Ren, X. Cai, W. Liu and J. Yao, ZIF-8 derived porous carbon to mitigate shuttle effect for high performance aqueous zinc–iodine batteries, *J. Colloid Interface Sci.*, 2022, **610**, 98–105.
22 H. X. Dang, A. J. Sellathurai and D. P. J. Barz, An ion exchange membrane-free, ultrastable zinc-iodine battery enabled by functionalized graphene electrodes, *Energy Storage Mater.*, 2023, **55**, 680–690.
23 S.-J. Zhang, J. Hao, H. Li, P.-F. Zhang, Z.-W. Yin, Y.-Y. Li, B. Zhang, Z. Lin and S.-Z. Qiao, Polyiodide Confinement by Starch Enables Shuttle-Free Zn–Iodine Batteries, *Adv. Mater.*, 2022, **34**, 2201716.
24 H. Peng, Y. Fang, J. Wang, P. Ruan, Y. Tang, B. Lu, X. Cao, S. Liang and J. Zhou, Constructing fast-ion-conductive disordered interphase for high-performance zinc-ion and zinc-iodine batteries, *Matter*, 2022, **5**, 4363–4378.

25 Y. Cui, Y. He, W. Yu, W. Shang, J. Yu and P. Tan, Tailoring the Electrochemical Deposition of Zn by Tuning the Viscosity of the Liquid Electrolyte, *ACS Appl. Mater. Interfaces*, 2023, **15**, 3028–3036.
26 H. Peng, C. Wang, D. Wang, X. Song, C. Zhang and J. Yang, Dynamic Zn/Electrolyte Interphase and Enhanced Cation Transfer of Sol Electrolyte for All-Climate Aqueous Zinc Metal Batteries, *Angew. Chem., Int. Ed.*, 2023, **62**, e202308068.
27 Q. Wen, H. Fu, R.-d. Cui, H.-Z. Chen, R.-H. Ji, L.-B. Tang, C. Yan, J. Mao, K.-H. Dai, X.-H. Zhang and J.-C. Zheng, Recent advances in interfacial modification of zinc anode for aqueous rechargeable zinc ion batteries, *J. Energy Chem.*, 2023, **83**, 287–303.
28 Q. Yang, Q. Li, Z. Liu, D. Wang, Y. Guo, X. Li, Y. Tang, H. Li, B. Dong and C. Zhi, Dendrites in Zn-Based Batteries, *Adv. Mater.*, 2020, **32**, 2001854.
29 J. Wang, Y. Yang, Y. Zhang, Y. Li, R. Sun, Z. Wang and H. Wang, Strategies towards the challenges of zinc metal anode in rechargeable aqueous zinc ion batteries, *Energy Storage Mater.*, 2021, **35**, 19–46.
30 Y. He, M. Liu and J. Zhang, Rational Modulation of Carbon Fibers for High-Performance Zinc–Iodine Batteries, *Adv. Sustainable Syst.*, 2020, **4**, 2000138.
31 L. Wu and Y. Dong, Recent progress of carbon nanomaterials for high-performance cathodes and anodes in aqueous zinc ion batteries, *Energy Storage Mater.*, 2021, **41**, 715–737.
32 L. Yan, T. Liu, X. Zeng, L. Sun, X. Meng, M. Ling, M. Fan and T. Ma, Multifunctional porous carbon strategy assisting high-performance aqueous zinc-iodine battery, *Carbon*, 2022, **187**, 145–152.
33 L. Chai, X. Wang, Y. Hu, X. Li, S. Huang, J. Pan, J. Qian and X. Sun, In-MOF-Derived Hierarchically Hollow Carbon Nanostraws for Advanced Zinc-Iodine Batteries, *Adv. Sci.*, 2022, **9**, 2105063.
34 S. Niu, B. Zhao and D. Liu, High-Performance Zn–I_2 Batteries Enabled by a Metal-Free Defect-Rich Carbon Cathode Catalyst, *ACS Appl. Mater. Interfaces*, 2023, **15**, 25558–25566.
35 W. Liu, P. Liu, Y. Lyu, J. Wen, R. Hao, J. Zheng, K. Liu, Y.-J. Li and S. Wang, Advanced Zn–I_2 Battery with Excellent Cycling Stability and Good Rate Performance by a Multifunctional Iodine Host, *ACS Appl. Mater. Interfaces*, 2022, **14**, 8955–8962.
36 Z. Gong, C. Song, C. Bai, X. Zhao, Z. Luo, G. Qi, X. Liu, C. Wang, Y. Duan and Z. Yuan, Anchoring high-mass iodine to nanoporous carbon with large-volume micropores and rich pyridine-N sites for high-energy-density and long-life Zn-I_2 aqueous battery, *Sci. China Mater.*, 2023, **66**, 556–566.
37 D. Yu, A. Kumar, T. A. Nguyen, M. T. Nazir and G. Yasin, High-Voltage and Ultrastable Aqueous Zinc–Iodine Battery Enabled by N-Doped Carbon Materials: Revealing the Contributions of Nitrogen Configurations, *ACS Sustainable Chem. Eng.*, 2020, **8**, 13769–13776.
38 J. Sun, H. Ma and D. Wang, Heavily heteroatoms doped carbons with tunable microstructure as the iodine hosts for rechargeable zinc-iodine aqueous batteries, *J. Alloys Compd.*, 2023, **947**, 169696.
39 J. Xu, W. Ma, L. Ge, M. Ren, X. Cai, W. Liu, J. Yao, C. Zhang and H. Zhao, Confining iodine into a biomass-derived hierarchically porous carbon as cathode material for high performance zinc–iodine battery, *J. Alloys Compd.*, 2022, **912**, 165151.
40 Y. Zhang, T. Zhao, S. Yang, Y. Zhang, Y. Ma and Z. Wang, Flexible PEDOT:PSS nanopapers as "anion-cation regulation" synergistic interlayers enabling ultra-stable aqueous zinc-iodine batteries, *J. Energy Chem.*, 2022, **75**, 310–320.
41 H. Yang, Y. Qiao, Z. Chang, H. Deng, P. He and H. Zhou, A Metal–Organic Framework as a Multifunctional Ionic Sieve Membrane for Long-Life Aqueous Zinc–Iodide Batteries, *Adv. Mater.*, 2020, **32**, 2004240.
42 H. K. Machhi, K. K. Sonigara, S. N. Bariya, H. P. Soni and S. S. Soni, Hierarchically Porous Metal–Organic Gel Hosting Catholyte for Limiting Iodine Diffusion and Self-Discharge Control in Sustainable Aqueous Zinc–I_2 Batteries, *ACS Appl. Mater. Interfaces*, 2021, **13**, 21426–21435.
43 X. Li, N. Li, Z. Huang, Z. Chen, G. Liang, Q. Yang, M. Li, Y. Zhao, L. Ma, B. Dong, Q. Huang, J. Fan and C. Zhi, Enhanced Redox Kinetics and Duration of Aqueous I_2/I^- Conversion Chemistry by MXene Confinement, *Adv. Mater.*, 2021, **33**, 2006897.
44 Y. Zhang, L. Wang, Q. Li, B. Hu, J. Kang, Y. Meng, Z. Zhao and H. Lu, Iodine Promoted Ultralow Zn Nucleation Overpotential and Zn-Rich Cathode for Low-Cost, Fast-Production and High-Energy Density Anode-Free Zn-Iodine Batteries, *Nano-Micro Lett.*, 2022, **14**, 208.
45 Y. Yang, S. Liang, B. Lu and J. Zhou, Eutectic electrolyte based on N-methylacetamide for highly reversible zinc–iodine battery, *Energy Environ. Sci.*, 2022, **15**, 1192–1200.
46 W. Li, K. Wang and K. Jiang, A high energy efficiency and long life aqueous Zn–I_2 battery, *J. Mater. Chem. A*, 2020, **8**, 3785–3794.
47 Q. Guo, H. Wang, X. Sun, Y. n. Yang, N. Chen and L. Qu, In Situ Synthesis of Cathode Materials for Aqueous High-Rate and Durable Zn–I_2 Batteries, *ACS Mater. Lett.*, 2022, **4**, 1872–1881.
48 Y. Hou, C. Zhu, Q. Wang, X. Zhao, K. Luo, Z. Gong and Z. Yuan, ~2.5 nm pores in carbon-based cathode promise better zinc-iodine batteries, *Chin. Chem. Lett.*, 2023, 108697, DOI: **10.1016/j.cclet.2023.108697**.
49 Y. Wu, Y. Qian, C. Huang, Y. Zhang, Y. Yang, A. Hu, Q. Tang and X. Chen, Hierarchical porous soft carbon host for the cathode of an aqueous zinc-iodine battery with ultra-long cycle life, *Electrochim. Acta*, 2023, **460**, 142593.
50 W. Han and X. Li, Electrode and electrolyte additive synergy effect for improving the capacity and supporting a high voltage plateau of aqueous rechargeable zinc iodine batteries, *J. Power Sources*, 2023, **580**, 233296.

51 Y. Gao, S. Gao, X. Pang, D. Chu, W. Zhu and J. Huang, Enhanced redox kinetics of iodine electrocatalyzed by cobalt (II) phthalocyanine for high-performance zinc-iodine battery, *Electrochim. Acta*, 2023, **464**, 142923.

52 T. Liu, H. Wang, C. Lei, Y. Mao, H. Wang, X. He and X. Liang, Recognition of the catalytic activities of graphitic N for zinc-iodine batteries, *Energy Storage Mater.*, 2022, **53**, 544–551.

53 Y. Kang, G. Chen, H. Hua, M. Zhang, J. Yang, P. Lin, H. Yang, Z. Lv, Q. Wu, J. Zhao and Y. Yang, A Janus Separator based on Cation Exchange Resin and Fe Nanoparticles-decorated Single-wall Carbon Nanotubes with Triply Synergistic Effects for High-areal Capacity Zn−I_2 Batteries, *Angew. Chem., Int. Ed.*, 2023, **62**, e202300418.

54 S. Ding, Q. Chen, S. Chen, Y. Tian and J. Zhang, The dispersion of iron nitride among porous carbon fibers to enhance redox conversion for high-performance zinc-iodine batteries, *Chin. Chem. Lett.*, 2023, **34**, 108232.

55 S. Chai, J. Yao, Y. Wang, J. Zhu and J. Jiang, Mediating iodine cathodes with robust directional halogen bond interactions for highly stable rechargeable Zn-I_2 batteries, *Chem. Eng. J.*, 2022, **439**, 135676.

56 L. Ma, G. Zhu, Z. Wang, A. Zhu, K. Wu, B. Peng, J. Xu, D. Wang and Z. Jin, Long-Lasting Zinc–Iodine Batteries with Ultrahigh Areal Capacity and Boosted Rate Capability Enabled by Nickel Single-Atom Electrocatalysts, *Nano Lett.*, 2023, **23**, 5272–5280.

57 X. Jin, L. Song, C. Dai, Y. Xiao, Y. Han, X. Li, Y. Wang, J. Zhang, Y. Zhao, Z. Zhang, N. Chen, L. Jiang and L. Qu, A Flexible Aqueous Zinc–Iodine Microbattery with Unprecedented Energy Density, *Adv. Mater.*, 2022, **34**, 2109450.

58 W. Wu, C. Li, Z. Wang, H.-Y. Shi, Y. Song, X.-X. Liu and X. Sun, Electrode and electrolyte regulation to promote coulombic efficiency and cycling stability of aqueous zinc-iodine batteries, *Chem. Eng. J.*, 2022, **428**, 131283.

59 J. Zhang, Q. Dou, C. Yang, L. Zang and X. Yan, Polyiodide shuttle inhibition in ethylene glycol-added aqueous electrolytes for high energy and long-term cyclability of zinc–iodine batteries, *J. Mater. Chem. A*, 2023, **11**, 3632–3639.

60 Y. Ji, J. Xie, Z. Shen, Y. Liu, Z. Wen, L. Luo and G. Hong, Advanced Zinc–Iodine Batteries with Ultrahigh Capacity and Superior Rate Performance Based on Reduced Graphene Oxide and Water-in-Salt Electrolyte, *Adv. Funct. Mater.*, 2023, **33**, 2210043.

61 Y. Liu, N. Chen, Z. Wang, S. Xu, D. Xiong, L. Wang, P. Yang and P. K. Chu, Stable static zinc-iodine redox battery constructed with graphene quantum dots coated graphite felt, *J. Power Sources*, 2022, **520**, 230861.

62 M. Chen, W. Zhu, H. Guo, Z. Tian, L. Zhang, J. Wang, T. Liu, F. Lai and J. Huang, Tightly confined iodine in surface-oxidized carbon matrix toward dual-mechanism zinc-iodine batteries, *Energy Storage Mater.*, 2023, **59**, 102760.

63 X. Zeng, X. Meng, W. Jiang, J. Liu, M. Ling, L. Yan and C. Liang, Anchoring Polyiodide to Conductive Polymers as Cathode for High-Performance Aqueous Zinc–Iodine Batteries, *ACS Sustainable Chem. Eng.*, 2020, **8**, 14280–14285.

64 X. Miao, Q. Chen, Y. Liu, X. Zhang, Y. Chen, J. Lin, S. Chen and Y. Zhang, Performance comparison of electro-polymerized polypyrrole and polyaniline as cathodes for iodine redox reaction in zinc-iodine batteries, *Electrochim. Acta*, 2022, **415**, 140206.

65 D. Zhao, Q. Zhu, Q. Zhou, W. Zhang, Y. Yu, S. Chen and Z. Ren, Enhancing I^0/I^- Conversion Efficiency by Starch Confinement in Zinc–Iodine Battery, *Energy Environ. Mater.*, 2022, e12522.

66 W. Gao, S. Cheng, Y. Zhang, E. Xie and J. Fu, Efficient Charge Storage in Zinc–Iodine Batteries based on Pre-Embedded Iodine-Ions with Reduced Electrochemical Reaction Barrier and Suppression of Polyiodide Self-Shuttle Effect, *Adv. Funct. Mater.*, 2023, **33**, 2211979.

67 W. Li, L. Huang, H. Zhang, Y. Wu, F. Wei, T. Zhang, J. Fu, C. Jing, J. Cheng and S. Liu, Supramolecular mineralization strategy for engineering covalent organic frameworks with superior Zn-I_2 battery performances, *Matter*, 2023, **6**, 2312–2323.

68 X. Li, M. Li, Z. Huang, G. Liang, Z. Chen, Q. Yang, Q. Huang and C. Zhi, Activating the I^0/I^+ redox couple in an aqueous I_2–Zn battery to achieve a high voltage plateau, *Energy Environ. Sci.*, 2021, **14**, 407–413.

69 S. Wang, Z. Huang, B. Tang, X. Li, X. Zhao, Z. Chen, C. Zhi and A. L. Rogach, Conversion-Type Organic-Inorganic Tin-Based Perovskite Cathodes for Durable Aqueous Zinc-Iodine Batteries, *Adv. Energy Mater.*, 2023, **13**, 2300922.

70 Z. Zhang, W. Ling, N. Ma, J. Wang, X. Chen, J. Fan, M. Yu and Y. Huang, Ultralong Cycle Life and High Rate of Zn‖I_2 Battery Enabled by MBene-Hosted I_2 Cathode, *Adv. Funct. Mater.*, 2024, **34**, 2310294.

71 F. Lanlan, L. Zhenhuan and D. Nanping, Recent advances in vanadium-based materials for aqueous metal ion batteries: Design of morphology and crystal structure, evolution of mechanisms and electrochemical performance, *Energy Storage Mater.*, 2021, **41**, 152–182.

72 D. Lin, D. Rao, S. Chiovoloni, S. Wang, J. Q. Lu and Y. Li, Prototypical Study of Double-Layered Cathodes for Aqueous Rechargeable Static Zn–I_2 Batteries, *Nano Lett.*, 2021, **21**, 4129–4135.

73 L. Zhang, M. Zhang, H. Guo, Z. Tian, L. Ge, G. He, J. Huang, J. Wang, T. Liu, I. P. Parkin and F. Lai, A Universal Polyiodide Regulation Using Quaternization Engineering toward High Value-Added and Ultra-Stable Zinc-Iodine Batteries, *Adv. Sci.*, 2022, **9**, 2105598.

74 Y. He, M. Liu, S. Chen and J. Zhang, Shapeable carbon fiber networks with hierarchical porous structure for high-performance Zn-I_2 batteries, *Sci. China Chem.*, 2022, **65**, 391–398.

75 Y. Hou, F. Kong, Z. Wang, M. Ren, C. Qiao, W. Liu, J. Yao, C. Zhang and H. Zhao, High performance rechargeable aqueous zinc-iodine batteries *via* a double iodine species fixation strategy with mesoporous carbon and modified separator, *J. Colloid Interface Sci.*, 2023, **629**, 279–287.

76 S. Chen, Q. Chen, J. Ma, J. Wang, K. S. Hui and J. Zhang, Interface Coordination Stabilizing Reversible Redox of Zinc for High-Performance Zinc-Iodine Batteries, *Small*, 2022, **18**, 2200168.

77 R. Yi, X. Shi, Y. Tang, Y. Yang, P. Zhou, B. Lu and J. Zhou, Carboxymethyl Chitosan-Modified Zinc Anode for High-Performance Zinc–Iodine Battery with Narrow Operating Voltage, *Small Struct.*, 2023, **4**, 2300020.

78 K. Wang, J.-B. Le, S.-J. Zhang, W.-F. Ren, J.-M. Yuan, T.-T. Su, B.-Y. Chi, C.-Y. Shao and R.-C. Sun, A renewable biomass-based lignin film as an effective protective layer to stabilize zinc metal anodes for high-performance zinc–iodine batteries, *J. Mater. Chem. A*, 2022, **10**, 4845–4857.

79 L. Zhang, J. Huang, H. Guo, L. Ge, Z. Tian, M. Zhang, J. Wang, G. He, T. Liu, J. Hofkens, D. J. L. Brett and F. Lai, Tuning Ion Transport at the Anode-Electrolyte Interface *via* a Sulfonate-Rich Ion-Exchange Layer for Durable Zinc-Iodine Batteries, *Adv. Energy Mater.*, 2023, **13**, 2203790.

80 T.-T. Su, J.-B. Le, K. Wang, K.-N. Liu, C.-Y. Shao, W.-F. Ren and R.-C. Sun, Tetraethyl orthosilicate steam induced silicon-based anticorrosion film enables highly reversible zinc metal anodes for zinc-iodine batteries, *J. Power Sources*, 2022, **550**, 232136.

81 P. Xue, C. Guo, L. Li, H. Li, D. Luo, L. Tan and Z. Chen, A MOF-Derivative Decorated Hierarchical Porous Host Enabling Ultrahigh Rates and Superior Long-Term Cycling of Dendrite-Free Zn Metal Anodes, *Adv. Mater.*, 2022, **34**, 2110047.

82 X. Wang, J. Meng, X. Lin, Y. Yang, S. Zhou, Y. Wang and A. Pan, Stable Zinc Metal Anodes with Textured Crystal Faces and Functional Zinc Compound Coatings, *Adv. Funct. Mater.*, 2021, **31**, 2106114.

83 W. Zhang, Y. Dai, R. Chen, Z. Xu, J. Li, W. Zong, H. Li, Z. Li, Z. Zhang, J. Zhu, F. Guo, X. Gao, Z. Du, J. Chen, T. Wang, G. He and I. P. Parkin, Highly Reversible Zinc Metal Anode in a Dilute Aqueous Electrolyte Enabled by a pH Buffer Additive, *Angew. Chem., Int. Ed.*, 2023, **62**, e202212695.

84 Y. Dai, C. Zhang, W. Zhang, L. Cui, C. Ye, X. Hong, J. Li, R. Chen, W. Zong, X. Gao, J. Zhu, P. Jiang, Q. An, D. J. L. Brett, I. P. Parkin, G. He and L. Mai, Reversible Zn Metal Anodes Enabled by Trace Amounts of Underpotential Deposition Initiators, *Angew. Chem., Int. Ed.*, 2023, **62**, e202301192.

85 D. Chao, W. Zhou, F. Xie, C. Ye, H. Li, M. Jaroniec and S.-Z. Qiao, Roadmap for advanced aqueous batteries: From design of materials to applications, *Sci. Adv.*, 2020, **6**, eaba4098.

86 L. Ma, S. Chen, N. Li, Z. Liu, Z. Tang, J. A. Zapien, S. Chen, J. Fan and C. Zhi, Hydrogen-Free and Dendrite-Free All-Solid-State Zn-Ion Batteries, *Adv. Mater.*, 2020, **32**, 1908121.

87 Q. Chen, S. Chen and J. Zhang, Interface engineering enables stable and reversible zinc anode for high-performance Zn–I_2 battery, *J. Power Sources*, 2023, **556**, 232529.

88 C. Chen, Z. Li, Y. Xu, Y. An, L. Wu, Y. Sun, H. Liao, K. Zheng and X. Zhang, High-Energy Density Aqueous Zinc–Iodine Batteries with Ultra-long Cycle Life Enabled by the ZnI_2 Additive, *ACS Sustainable Chem. Eng.*, 2021, **9**, 13268–13276.

89 G. Chen, Y. Kang, H. Yang, M. Zhang, J. Yang, Z. Lv, Q. Wu, P. Lin, Y. Yang and J. Zhao, Toward Forty Thousand-Cycle Aqueous Zinc-Iodine Battery: Simultaneously Inhibiting Polyiodides Shuttle and Stabilizing Zinc Anode through a Suspension Electrolyte, *Adv. Funct. Mater.*, 2023, **33**, 2300656.

90 G. Liang, B. Liang, A. Chen, J. Zhu, Q. Li, Z. Huang, X. Li, Y. Wang, X. Wang, B. Xiong, X. Jin, S. Bai, J. Fan and C. Zhi, Development of rechargeable high-energy hybrid zinc-iodine aqueous batteries exploiting reversible chlorine-based redox reaction, *Nat. Commun.*, 2023, **14**, 1856.

91 K. K. Sonigara, J. Zhao, H. K. Machhi, G. Cui and S. S. Soni, Self-Assembled Solid-State Gel Catholyte Combating Iodide Diffusion and Self-Discharge for a Stable Flexible Aqueous Zn–I_2 Battery, *Adv. Energy Mater.*, 2020, **10**, 2001997.

92 W. Shang, J. Zhu, Y. Liu, L. Kang, S. Liu, B. Huang, J. Song, X. Li, F. Jiang, W. Du, Y. Gao and H. Luo, Establishing High-Performance Quasi-Solid Zn/I_2 Batteries with Alginate-Based Hydrogel Electrolytes, *ACS Appl. Mater. Interfaces*, 2021, **13**, 24756–24764.

93 S. Lv, T. Fang, Z. Ding, Y. Wang, H. Jiang, C. Wei, D. Zhou, X. Tang and X. Liu, A High-Performance Quasi-Solid-State Aqueous Zinc–Dual Halogen Battery, *ACS Nano*, 2022, **16**, 20389–20399.

94 Y. Tian, S. Chen, S. Ding, Q. Chen and J. Zhang, A highly conductive gel electrolyte with favorable ion transfer channels for long-lived zinc–iodine batteries, *Chem. Sci.*, 2023, **14**, 331–337.

95 J. Hao, L. Yuan, Y. Zhu, X. Bai, C. Ye, Y. Jiao and S.-Z. Qiao, Low-cost and Non-flammable Eutectic Electrolytes for Advanced Zn-I_2 Batteries, *Angew. Chem., Int. Ed.*, 2023, **62**, e202310284.

96 C. Li, R. Kingsbury, A. S. Thind, A. Shyamsunder, T. T. Fister, R. F. Klie, K. A. Persson and L. F. Nazar, Enabling selective zinc-ion intercalation by a eutectic electrolyte for practical anodeless zinc batteries, *Nat. Commun.*, 2023, **14**, 3067.

97 S. Jin, D. Zhang, A. Sharma, Q. Zhao, Y. Shao, P. Chen, J. Zheng, J. Yin, Y. Deng, P. Biswal and L. A. Archer, Stabilizing Zinc Electrodeposition in a Battery Anode by Controlling Crystal Growth, *Small*, 2021, **17**, 2101798.

98 Q. Yang, L. Li, T. Hussain, D. Wang, L. Hui, Y. Guo, G. Liang, X. Li, Z. Chen, Z. Huang, Y. Li, Y. Xue, Z. Zuo, J. Qiu, Y. Li and C. Zhi, Stabilizing Interface pH by N-Modified Graphdiyne for Dendrite-Free and High-Rate Aqueous Zn-Ion Batteries, *Angew. Chem., Int. Ed.*, 2022, **61**, e202112304.

99 F. Mo, Z. Chen, G. Liang, D. Wang, Y. Zhao, H. Li, B. Dong and C. Zhi, Zwitterionic Sulfobetaine Hydrogel Electrolyte Building Separated Positive/Negative Ion Migration Channels for Aqueous Zn-MnO_2 Batteries with Superior Rate Capabilities, *Adv. Energy Mater.*, 2020, **10**, 2000035.

100 J. J. Hong, L. Zhu, C. Chen, L. Tang, H. Jiang, B. Jin, T. C. Gallagher, Q. Guo, C. Fang and X. Ji, A Dual Plating Battery with the Iodine/$[ZnI_x(OH_2)_{4-x}]_{2-x}$ Cathode, *Angew. Chem., Int. Ed.*, 2019, **58**, 15910–15915.

101 Z. Yi, G. Chen, F. Hou, L. Wang and J. Liang, Strategies for the Stabilization of Zn Metal Anodes for Zn-Ion Batteries, *Adv. Energy Mater.*, 2021, **11**, 2003065.

102 S.-J. Zhang, J. Hao, Y. Zhu, H. Li, Z. Lin and S.-Z. Qiao, pH-Triggered Molecular Switch Toward Texture-Regulated Zn Anode, *Angew. Chem., Int. Ed.*, 2023, **62**, e202301570.

103 Z. Khan, D. Kumar and X. Crispin, Does Water-in-Salt Electrolyte Subdue Issues of Zn Batteries?, *Adv. Mater.*, 2023, **35**, 2300369.

104 Q. Liu, C. Xia, C. He, W. Guo, Z. P. Wu, Z. Li, Q. Zhao and B. Y. Xia, Dual-Network Structured Hydrogel Electrolytes Engaged Solid-State Rechargeable Zn-Air/Iodide Hybrid Batteries, *Angew. Chem., Int. Ed.*, 2022, **61**, e202210567.

105 J. Shi, T. Sun, J. Bao, S. Zheng, H. Du, L. Li, X. Yuan, T. Ma and Z. Tao, "Water-in-Deep Eutectic Solvent" Electrolytes for High-Performance Aqueous Zn-Ion Batteries, *Adv. Funct. Mater.*, 2021, **31**, 2102035.

106 B. B. Hansen, S. Spittle, B. Chen, D. Poe, Y. Zhang, J. M. Klein, A. Horton, L. Adhikari, T. Zelovich, B. W. Doherty, B. Gurkan, E. J. Maginn, A. Ragauskas, M. Dadmun, T. A. Zawodzinski, G. A. Baker, M. E. Tuckerman, R. F. Savinell and J. R. Sangoro, Deep Eutectic Solvents: A Review of Fundamentals and Applications, *Chem. Rev.*, 2021, **121**, 1232–1285.

107 A. P. Abbott, J. C. Barron, K. S. Ryder and D. Wilson, Eutectic-Based Ionic Liquids with Metal-Containing Anions and Cations, *Chem.–Eur. J.*, 2007, **13**, 6495–6501.

108 S.-B. Wang, Q. Ran, R.-Q. Yao, H. Shi, Z. Wen, M. Zhao, X.-Y. Lang and Q. Jiang, Lamella-nanostructured eutectic zinc–aluminum alloys as reversible and dendrite-free anodes for aqueous rechargeable batteries, *Nat. Commun.*, 2020, **11**, 1634.

109 X. Zeng, J. Hao, Z. Wang, J. Mao and Z. Guo, Recent progress and perspectives on aqueous Zn-based rechargeable batteries with mild aqueous electrolytes, *Energy Storage Mater.*, 2019, **20**, 410–437.

110 D. Chao and S.-Z. Qiao, Toward High-Voltage Aqueous Batteries: Super- or Low-Concentrated Electrolyte?, *Joule*, 2020, **4**, 1846–1851.

111 Z. Li, X. Wu, X. Yu, S. Zhou, Y. Qiao, H. Zhou and S.-G. Sun, Long-Life Aqueous Zn–I_2 Battery Enabled by a Low-Cost Multifunctional Zeolite Membrane Separator, *Nano Lett.*, 2022, **22**, 2538–2546.